

---

## Structure, transports and transformations of the water masses in the Atlantic Subpolar Gyre

Garcia-Ibanez Maribel I.<sup>1,\*</sup>, Pardo Paula C.<sup>1</sup>, Carracedo Lidia<sup>1</sup>, Mercier Herlé<sup>2</sup>, Lherminier Pascale<sup>3</sup>, Rios Aida F.<sup>1</sup>, Pérez Fiz F.<sup>1</sup>

<sup>1</sup> CSIC, Inst Invest Marinas, Vigo 36208, Spain.

<sup>2</sup> Ifremer Ctr Brest, CNRS, Lab Phys Oceans, UMR CNRS Ifremer IRD UBO 6523, Plouzane, France.

<sup>3</sup> Ifremer, Lab Phys Oceans, UMR CNRS Ifremer IRD UBO 6523, Plouzane, France.

\* Corresponding author : Maribel I. Garcia-Ibanez, email address : [maribelgarcia@iim.csic.es](mailto:maribelgarcia@iim.csic.es) ; [pconde@iim.csic.es](mailto:pconde@iim.csic.es) ; [lcarracedo@iim.csic.es](mailto:lcarracedo@iim.csic.es) ; [Herle.Mercier@ifremer.fr](mailto:Herle.Mercier@ifremer.fr) ; [Pascale.Lherminier@ifremer.fr](mailto:Pascale.Lherminier@ifremer.fr) ; [aida@iim.csic.es](mailto:aida@iim.csic.es) ; [fiz.perez@iim.csic.es](mailto:fiz.perez@iim.csic.es)

---

### Abstract :

We discuss the distributions and transports of the main water masses in the North Atlantic Subpolar Gyre (NASPG) for the mean of the period 2002–2010 (OVIDE sections 2002–2010 every other year), as well as the inter-annual variability of the water mass structure from 1997 (4x and METEOR sections) to 2010. The water mass structure of the NASPG, quantitatively assessed by means of an Optimum MultiParameter analysis (with 14 water masses), was combined with the velocity fields resulting from previous studies using inverse models to obtain the water mass volume transports. We also evaluate the relative contribution to the Atlantic Meridional Overturning Circulation (AMOC) of the main water masses characterizing the NASPG, identifying the water masses that contribute to the AMOC variability. The reduction of the magnitude of the upper limb of the AMOC between 1997 and the 2000s is associated with the reduction in the northward transport of the Central Waters. This reduction of the northward flow of the AMOC is partially compensated by the reduction of the southward flow of the lower limb of the AMOC, associated with the decrease in the transports of Polar Intermediate Water and Subpolar Mode Water (SPMW) in the Irminger Basin. We also decompose the flow over the Reykjanes Ridge from the East North Atlantic Basin to the Irminger Basin ( $9.4 \pm 4.7$  Sv) into the contributions of the Central Waters ( $2.1 \pm 1.8$  Sv), Labrador Sea Water (LSW,  $2.4 \pm 2.0$  Sv), Subarctic Intermediate Water (SAIW,  $4.0 \pm 0.5$  Sv) and Iceland–Scotland Overflow Water (ISOW,  $0.9 \pm 0.9$  Sv). Once LSW and ISOW cross over the Reykjanes Ridge, favoured by the strong mixing around it, they leave the Irminger Basin through the deep-to-bottom levels. The results also give insights into the water mass transformations within the NASPG, such as the contribution of the Central Waters and SAIW to the formation of the different varieties of SPMW due to air–sea interaction.

---

## Highlights

► We discuss the 1997–2010 water mass structure and transport of the WOCE A25 line. ► We combine OMP analysis with velocity fields. ► The Central Waters transport reduction is linked to the AMOC decline. ► The weakening of intermediate water transports partially balances the AMOC decline. ► Water masses exchanges across the Reykjanes Ridge were also evaluated.

## List of acronyms

AMOC	Atlantic Meridional Overturning Circulation
CGFZ	Charlie–Gibbs Fracture Zone
CTD	Conductivity-Temperature-Depth
DSOW	Denmark Strait Overflow Water
ENA	East North Atlantic (Basin)
ENACW	East North Atlantic Central Water
ISOW	Iceland–Scotland Overflow Water
LSW	Labrador Sea Water
MW	Mediterranean Water
NAC	North Atlantic Current
NADW	North Atlantic Deep Water
NAO	North Atlantic Oscillation
NASPG	North Atlantic Subpolar Gyre
NEADW	North East Atlantic Deep Water, upper (NEADW <sub>U</sub> ) and lower (NEADW <sub>L</sub> )
OMP	Optimum MultiParameter, classical (cOMP) and extended (eOMP)
OVIDE	Observatoire de la variabilité interannuelle et décennale en Atlantique Nord
PIW	Polar Intermediate Water
SAIW	Subarctic Intermediate Water
SPMW	Subpolar Mode Water, in the Iceland (IcSPMW) and Irminger (IrSPMW) Basins
SWT	Source Water Type
WOCE	World Ocean Circulation Experiment

## 74 **1. Introduction**

75           The North Atlantic Subpolar Gyre (NASPG) is one of the key regions of the global ocean  
76 circulation, where interactions with the atmosphere contribute to warm-to-cold water mass  
77 transformations (e.g., Bersch et al., 2007; Yashayaev et al., 2007; Sarafanov, 2009; Sarafanov et  
78 al., 2012). The North Atlantic Current (NAC) carries warm and salty waters from the subtropics  
79 towards the north-eastern Atlantic Ocean (Fig. 1). East of the Charlie–Gibbs Fracture Zone (CGFZ)  
80 the NAC bifurcates into two branches, one flowing towards the Nordic Seas, and the other flowing  
81 towards the Iceland Basin (Read, 2000), where the Subpolar Mode Water (SPMW) is formed  
82 (McCartney and Talley, 1982; Tsuchiya et al., 1992; van Aken and Becker, 1996; Brambilla and  
83 Talley, 2008). The densest variety of SPMW is formed in the Labrador Sea (McCartney and Talley,  
84 1982; Yashayaev, 2007), where intense winter heat loss leads to deep convection and formation of  
85 the Labrador Sea Water (LSW) (Tsuchiya et al., 1992; Bersch et al., 2007; Yashayaev, 2007).  
86 Afterwards, LSW joins the Deep Western Boundary Current (Bersch et al., 2007), where it flows  
87 over the Denmark Strait Overflow Water (DSOW) and the Iceland–Scotland Overflow Water  
88 (ISOW) (both derived from waters from the Arctic Ocean and the Nordic Seas; Rudels et al., 2002;  
89 Tanhua et al., 2008) and these altogether constitute the North Atlantic Deep Water (NADW;  
90 Dickson and Brown, 1994).

91           The processes of water mass formation in the Subpolar North Atlantic, the Arctic Ocean  
92 and the Nordic Seas affect the Atlantic Meridional Overturning Circulation (AMOC) on long  
93 timescales (Böning et al., 1996; Willebrand et al., 2001; Marsh et al., 2005; Josey et al., 2009). The  
94 AMOC transports heat and anthropogenic carbon from the southern hemisphere of the Atlantic  
95 Ocean to the subtropics and the high northern latitudes, playing an active role in the climate  
96 variability. The North Atlantic Oscillation (NAO) is the dominant mode of the atmospheric variability  
97 in the NASPG (Hurrell, 1995), which influences both its strength and circulation (Curry and  
98 McCartney, 2001; Häkkinen and Rhines, 2004) and its shape (Bersch, 2002). Both direct  
99 observations (Flatau et al., 2003; Häkkinen and Rhines, 2004) and model results (Böning et al.,  
100 2006) confirm a spin down of the circulation of the NASPG between the mid-1990s and the 2000s  
101 due to the shift from high to low NAO indices, based on high-frequency time series. The NAO also  
102 influences the AMOC strength (e.g., Eden and Willebrand, 2001; Marsh et al., 2005; Böning et al.,

103 2006; Balmaseda et al., 2007), which has decreased over the last decade (Balmaseda et al., 2007;  
104 Desbruyères et al., 2013; Xu et al., 2013; Mercier et al., 2015) and resulted in reductions in the  
105 poleward heat transport (Bryden et al., 2014; Mercier et al., 2015) and in the uptake of atmospheric  
106 carbon dioxide (Pérez et al., 2013).

107 The main objective of this paper is to discuss the distributions and transports of the main  
108 water masses in the North Atlantic region for the first decade of the 2000s. We also evaluate the  
109 inter-annual variability of the water mass structure from 1997 to 2010. In the present work we use  
110 data from six repeats of the WOCE (World Ocean Circulation Experiment) A25 hydrographic  
111 section located at the southern boundary of the NASPG (Fig. 1; Table 1). The data include the 4x  
112 section taken in 1997 and the five repeats of the OVIDE (Observatoire de la variabilité  
113 interannuelle et décennale en Atlantique Nord) section taken every other year from 2002 to 2010.  
114 We obtained the distributions of the main water masses in each section by using an Optimum  
115 MultiParameter (OMP) analysis (Thompson and Edwards, 1981; Tomczak, 1981; Mackas et al.,  
116 1987; Tomczak and Large, 1989) and then we combined them with the velocity fields (from inverse  
117 models previously implemented (Lherminier et al., 2007, 2010; Gourcuff et al., 2011; Mercier et al.,  
118 2015)) in order to estimate the transport of each water mass across the sections. Although this  
119 methodology has been applied before (Álvarez et al., 2004; Carracedo et al., 2014), this is the first  
120 time that it has been used to evaluate the inter-annual variability of the water mass distributions,  
121 specifically from 1997 to 2010. In addition, we also investigate the water mass contributions to the  
122 AMOC and the water mass transformations that take place in the NASPG.

123 The present manuscript is organized as follows. In Section 2 we describe: the cruise data;  
124 the methodology followed in the OMP analysis, including a description of the 14 water masses  
125 considered; the velocity field obtained from earlier studies; and the methodology used to combine  
126 the velocity fields with the water mass distributions. The water mass distributions for the OVIDE  
127 period (2002–2010) are described and discussed in Section 3. In Section 4 we describe and  
128 discuss the inter-annual variability of the water mass structure from 1997 to 2010. The water mass  
129 volume transports are described and discussed in Section 5 together with an estimation of the  
130 circulation and transformation of the water masses in the Subpolar North Atlantic as well as of the

131 budget of water mass volume transports across the Reykjanes Ridge. We conclude the manuscript  
132 in Section 6.

## 133 **2. Data and methods**

### 134 **2.1. Biogeochemical data**

135 The 4x and OVIDE sections were conducted across the southern boundary of the NASPG  
136 from the Iberian Peninsula to Cape Farewell (South Greenland), during the spring–summer periods  
137 of 1997 (4x section), 2002, 2004, 2006, 2008 and 2010 (OVIDE sections) (Fig. 1; Table 1). Cruise  
138 data is available on the CCHDO (CLIVAR & Carbon Hydrographic Data Office) webpage  
139 (<http://cchdo.ucsd.edu>). These cruises are suitable for examining the inter-annual to decadal water  
140 mass variability because they were carried out at approximately the same time of the year -from  
141 June to August- and, except for the near-surface layers, the seasonal differences are expected to  
142 be smaller than the inter-annual changes. In addition, the monthly variability of the AMOC is  
143 weaker between June and August (Mercier et al., 2015).

144 During the cruises, the temperature and salinity (S) were continuously recorded at each  
145 station by using a Conductivity–Temperature–Depth (CTD) instrument. In the cruises prior to 2008  
146 a Neil Brown Mark III CTD probe was used, while in the subsequent cruises a Sea-bird Electronics  
147 911plus CTD probe was used. To calibrate the conductivity sensor, seawater S samples were  
148 analysed on board via a Guildline 8400A salinometer calibrated with IAPSO Standard Seawater  
149 following the WOCE standards (Culberson, 1991). The pressure sensor was calibrated in a  
150 metrology laboratory using 3 cycles of increasing–decreasing pressure between 0 and 6000 dbar.  
151 The static and dynamic effects of temperature on the pressure sensor were also estimated and  
152 corrected (Branellec and Thierry, 2013). Overall, the CTD measurement accuracies were 1 dbar  
153 for pressure, 0.002°C for temperature and 0.003 for S.

154 Seawater samples for nutrients (nitrate (NO<sub>3</sub>), phosphate (PO<sub>4</sub>) and silicate (SiO<sub>2</sub>)) and  
155 oxygen (O<sub>2</sub>) were also taken and analysed on board. The nutrients were analysed using an SOC  
156 Chemlab AAll type Auto-Analyser coupled with a Digital-Analysis Microstream data capture and a  
157 reduction system, following the classic protocols and methods described by Aminot and

158 Chaussepied (1983). The precision for  $\text{NO}_3$ ,  $\text{PO}_4$  and  $\text{SiO}_2$  was evaluated at 0.2, 0.02 and 0.1  $\mu\text{mol}$   
159  $\text{kg}^{-1}$ , respectively. The  $\text{O}_2$  was determined by Winkler potentiometric titration following the WOCE  
160 standards (Culberson, 1991), with a precision better than  $\mu\text{mol kg}^{-1}$ .

161 For further reference, the vertical sections of the mean properties (potential temperature  
162  $(\theta)$ , S,  $\text{O}_2$ ,  $\text{NO}_3$ ,  $\text{SiO}_2$  and  $\text{PO}_4$ ) are shown in Fig. 2.

## 163 **2.2. Optimum MultiParameter (OMP) analysis**

164 An Optimum MultiParameter (OMP) analysis (Thompson and Edwards, 1981; Tomczak,  
165 1981; Mackas et al., 1987; Tomczak and Large, 1989) was used to resolve the water mass  
166 structure along the sections. The water masses are described by the so-called Source Water  
167 Types (SWT), which are points in the  $n$ -dimensional parameter space ( $n$  is the number of  
168 properties that characterize SWTs) (Tomczak, 1999). In this work, the SWTs are characterized by  
169  $\theta$ , S,  $\text{O}_2^0$ ,  $\text{NO}_3^0$ ,  $\text{PO}_4^0$  and  $\text{SiO}_2^0$  (where the superscript 0 means preformed variables) (Table 2). Given  
170 a number of SWTs, the goal of an OMP analysis is to find the fractions of each SWT ( $X_i$ ) in each  
171 water sample. The  $X_i$ s strongly depend on the characterization of the SWTs (Tomczak, 1981), the  
172 choice of which is a key step of the analysis. In the following subsection we describe the SWTs  
173 included in the analysis and their properties.

### 174 **2.2.1. Water mass characterization**

175 The Subpolar North Atlantic is a region with a large variety of water masses. We considered  
176 14 SWTs as the main water masses explaining the physicochemical variability of this area and  
177 which encompass all the water samples of the sections (Fig. 3a, b).

178 The saltiest waters of the sections are influenced by the Mediterranean Water (MW), which  
179 enters the North Atlantic from the Mediterranean Sea. MW is detected as a maximum in S ( $> 36.1$ )  
180 and  $\theta$  (9-11°C) between 600 and 1700 m depth in the eastern North Atlantic (Harvey, 1982;  
181 Tsuchiya et al., 1992; van Aken and Becker, 1996; Álvarez et al., 2004). Following Castro et al.  
182 (1998) and Álvarez et al. (2004), we used the  $\theta$ /S properties of MW reported by Wüst and Defant  
183 (1936) near Cape St. Vicente (Fig. 3a; Table 2). In this way we avoid solving the mixing processes

184 between the Mediterranean Outflow Water (overflowing from the Mediterranean Sea) and the  
185 central and intermediate waters of the East North Atlantic, which lead to the formation of MW  
186 (Ambar and Howe, 1979; Baringer and Price, 1997).

187 The warmer waters are influenced by the North Atlantic Central Waters (Iselin, 1936). East  
188 of the Mid-Atlantic Ridge in the North Atlantic, the predominant variety of these waters is the East  
189 North Atlantic Central Water (ENACW) (Harvey, 1982; Pollard et al., 1996; Read, 2000), which is  
190 formed by winter convection in the intergyre region (Pollard et al., 1996). The  $\theta/S$  characteristics of  
191 ENACW can be fitted to a straight line from 12 to 16°C (Pollard et al., 1996). The end points from  
192 this line are defined by: ENACW<sub>16</sub>, whose  $\theta/S$  characteristics match those from the warmer central  
193 waters of Pollard et al. (1996); and ENACW<sub>12</sub>, which represents the upper limit of ENACW defined  
194 by Harvey (1982) (Fig. 3a; Table 2). Here, we considered these two SWTs together as the Central  
195 Waters.

196 Part of the Central Waters carried by the NAC recirculates in the West European Basin  
197 (Fig. 1), and part of them spreads towards the Iceland Basin, leading to the formation of SPMW  
198 (McCartney and Talley, 1982; Tsuchiya et al., 1992; van Aken and Becker, 1996; Brambilla and  
199 Talley, 2008). The hydrographic properties of SPMW change due to air–sea interaction processes  
200 (McCartney and Talley, 1982; Brambilla and Talley, 2008). Since this variability cannot be  
201 accounted by the OMP analysis, we defined three SWTs to characterize SPMW: two  
202 corresponding to SPMW present in the Iceland Basin (SPMW<sub>8</sub> and SPMW<sub>7</sub>), and another one that  
203 accounts for the variety found in the Irminger Basin (IrSPMW, sometimes denoted as Irminger Sea  
204 Water (Krauss, 1995)). SPMW<sub>8</sub> and SPMW<sub>7</sub> were selected to characterize the thermohaline range  
205 of SPMW in the Iceland Basin (6–9°C and 35.1–35.25) (Stoll et al., 1996; van Aken and Becker,  
206 1996) and are going to be considered together as IcSPMW. The  $\theta/S$  properties of SPMW<sub>7</sub> (Fig. 3a;  
207 Table 2) were chosen close to the mean properties of SPMW over the eastern flank of the  
208 Reykjanes Ridge found by Thierry et al. (2008) in a box including the OVIDE section, while the  $\theta/S$   
209 properties of SPMW<sub>8</sub> correspond to the SPMW variety formed within the Iceland Basin (Brambilla  
210 and Talley, 2008). Since the 8°C limit between the Central Waters and SPMW<sub>8</sub> (Brambilla and  
211 Talley, 2008; Brambilla et al., 2008) cannot be directly obtained by the OMP analysis, we  
212 constrained the OMP by not allowing the presence of Central Waters east of the western branch of

213 the NAC (Fig. 1). In the northern part of the Irminger Basin, SPMW is characterized by  $\theta$  and S  
214 usually lower than 7°C and 35.1, respectively (Thierry et al., 2008). To characterize the SWT for  
215 IrSPMW, we chose its  $\theta/S$  properties close to those of the Irminger Sea Water described by Krauss  
216 (1995) (Fig. 3a; Table 2). These properties were also found by Brambilla and Talley (2008) in the  
217 NW Irminger Basin, which could indicate that this is the region of formation of IrSPMW.

218 Once SPMW reaches the Labrador Sea, it is involved in deep convection processes which  
219 lead to the formation of LSW (Talley and McCartney, 1982). These episodes of deep convection  
220 are forced by the extreme winter heat loss combined with the cyclonic circulation in the Labrador  
221 Sea (Lazier et al., 2002). LSW is traceable by its low potential vorticity, relatively low S and high O<sub>2</sub>  
222 content (Fig. 2) (Talley and McCartney, 1982; Harvey and Arhan, 1988; Pickart, 1992; Tsuchiya et  
223 al., 1992). The classical LSW (Bersch et al., 2007; Yashayaev et al., 2008) is built by intense  
224 winter convection, when the mixing layer reaches ~2000 m depth. Deep winter convection at these  
225 latitudes is controlled by the phase of the NAO and its persistence (Dickson et al., 1996; Bersch et  
226 al., 2007). Indeed, it is favoured during persistent phases of the high NAO index, such as the  
227 period 1987–1994, when the winter convection reached 2400 m depth (Lazier et al., 2002;  
228 Yashayaev, 2007), where the LSW properties reached extremal values of 2.9°C and 34.84  
229 (Álvarez et al., 2004; Yashayaev, 2007). The thermohaline properties of the corresponding SWT  
230 are consistent with the characteristic values for the classical LSW as a long-term average (Lazier,  
231 1973; Dickson et al., 1996) (Fig. 3a, b; Table 2).

232 The left limit of the  $\theta/S$ -diagram is characterized by the Subarctic Intermediate Water  
233 (SAIW), which originates in the western boundary of the NASPG (Arhan, 1990) from the mixture of  
234 the warm and salty waters of the NAC with the cold and low-salinity waters of the Labrador Current  
235 (Iselin, 1936; Read, 2000). The thermohaline properties of SAIW (4-7°C and S < 34.9) vary due to  
236 its spreading and subduction in a region characterized by a complex circulation, with horizontal and  
237 vertical mixing, recirculation processes and mesoscale variability, among other processes  
238 (Bubnov, 1968; Arhan, 1990). Similarly to what we did in the case of SPMW and in order to better  
239 depict SAIW, we defined two SWTs: SAIW<sub>6</sub>, which represents the fresher and relatively warm  
240 variety resulting from the progressive warming of the fresher Arctic waters while mixing with central  
241 waters (Fig. 3a; Table 2); and SAIW<sub>4</sub>, which represents the saltier and relatively cold variety

242 resulting from the cooling of the saltier central waters while mixing with the Arctic waters. The  
243 thermohaline properties of both SWTs follow the descriptions of Bubnov (1968) and Harvey and  
244 Arhan (1988).

245 The bottom part of the  $\theta/S$ -diagram shows DSOW and ISOW, which are complex mixtures  
246 of several water masses. The Norwegian Sea waters overflow and entrain the overlying warm  
247 saline Atlantic waters (SPMW and LSW) forming ISOW (van Aken and de Boer, 1995; Dickson et  
248 al., 2002; Fogelqvist et al., 2003). To avoid the parameterization of this mixing process (as in the  
249 case of MW), we defined the ISOW thermohaline properties by considering this overflow as the  
250 final result of those mixing processes, and according to the definition of van Aken and Becker  
251 (1996) (Fig. 3a, b; Table 2). As for DSOW, it is formed after the Nordic Seas deep waters overflow  
252 and entrain Atlantic waters (SPMW and LSW) (Read, 2000; Yashayaev and Dickson, 2008). In  
253 addition, some authors have reported dense Greenland shelf water cascading down to the DSOW  
254 layer in the Irminger Sea (Olsson et al., 2005; Tanhua et al., 2005, 2008; Falina et al., 2012).  
255 According to this and following van Aken and de Jong (2012), we modelled DSOW by two SWTs: a  
256 relatively saline one (DSOW) and a relatively fresh one (the Polar Intermediate Water; PIW) (Fig.  
257 3a, b; Table 2). The  $\theta/S$  characteristics chosen for DSOW are in agreement with the characteristics  
258 of the saline variety of van Aken and de Jong (2012) and with the characteristics of DSOW after  
259 crossing the sill found by Tanhua et al. (2005). PIW is an SWT with characteristics close to the low-  
260 salinity variety of the overflow (Tanhua et al., 2005). We substituted the relatively fresh end-  
261 member proposed by van Aken and de Jong (2012) by PIW to take into account the dense shelf  
262 water intrusions, since these intrusions lie on a mixing line between PIW and the Irminger Current  
263 Water (Rudels et al., 2002; Falina et al., 2012). The  $\theta/S$  characteristics selected for PIW are in  
264 agreement with those proposed by Malmberg (1972) and Rudels et al. (2002).

265 The North East Atlantic Deep Water (NEADW) is formed as a result of different  
266 entrainments that occur along the journey of ISOW through the Iceland Basin (van Aken, 2000).  
267 NEADW recirculates in the Iberian Basin and mixes with the surrounding waters, including the  
268 bottom waters coming from the Southern Ocean (Antarctic Bottom Water; van Aken and Becker,  
269 1996). The  $\theta/S$  properties of NEADW below 2500 m depth in this basin can be approximated as a  
270 line (Saunders, 1986; Mantyla, 1994) whose end points define our SWTs representing the upper

271 (NEADW<sub>U</sub>) and lower (NEADW<sub>L</sub>) varieties of NEADW (Fig. 3a, b; Table 2). The  $\theta/S$  properties of  
272 these two SWTs are close to those defined by Castro et al. (1998).

273 Having selected the  $\theta/S$  properties for each SWT from the literature, we run the OMP  
274 analysis taking the remaining chemical properties ( $NO_3^0$ ,  $PO_4^0$  and  $SiO_2^0$ ) from the work of Álvarez et  
275 al. (2004) and the  $O_2^0$  equal to saturation as a first guess. For those SWTs not defined in Álvarez et  
276 al. (2004), their first-guess chemical properties were taken as equal to those properties of the  
277 nearest SWT in Álvarez et al. (2004) ( $O_2^0$  equal to saturation). The final chemical properties for  
278 each SWT (those that best fit the measured data) were obtained from an iterative procedure  
279 (section 2.2.2). Some of the values of  $O_2^0$  were adjusted so as not to get negative values for either  
280 respiration or nutrients, and to account for the disequilibrium between the  $O_2$  content in the  
281 atmosphere and in the water mass at its time of formation (in the surface ocean) (Najjar and  
282 Keeling, 2000; Ito et al., 2004). The uncertainties in the properties were obtained as explained in  
283 section A2 of the Appendix.

#### 284 2.2.2. Methodology of the analysis

285 An OMP analysis is a simple mathematical approach based on measured data that solves  
286 the mixing between SWTs by a least square method constrained to be positive definite (section A1  
287 of the Appendix). The methodology applied in this work consists of two steps (Pardo et al., 2012).  
288 First, the 14 SWTs were grouped into a total of 11 mixing *figures* (Fig. 3c), which are subsets of  
289 SWTs that are susceptible to mixing. The term *figure* refers to the geometrical space in the  $\theta/S$   
290 plane formed by 2 SWTs (line segment), 3 SWTs (triangle), 4 SWTs (square), etc. Actually, the  
291 mixing *figures* are  $n$ -dimensional spaces. These mixing *figures* were selected based on the  
292 characteristics and/or dynamics of the SWTs in the region of study. In the first step of the  
293 methodology we solved a classical OMP (cOMP) analysis (Tomczak, 1981), which is based only  
294 on conservative variables ( $\theta$ , S,  $SiO_2$ , “NO” and “PO”; see section A1 of the Appendix), for each  
295 water sample in each one of the mixing *figures*. In this way we assigned to each water sample the  
296 mixing *figure* whose mixing best explains its properties. In the second step we solved an extended  
297 OMP (eOMP) analysis to obtain the  $X_i$ s in each water sample for the mixing *figure* selected in the

298 previous step. The eOMP analysis includes conservative ( $\theta$  and S) and non-conservative ( $\text{NO}_3$ ,  
299  $\text{PO}_4$ ,  $\text{SiO}_2$  and  $\text{O}_2$ ) variables. By taking into account the biogeochemical process of remineralisation  
300 of the organic matter, we can include non-conservative variables (for more details about the  
301 methodology see section A1 of the Appendix). We restricted the whole OMP analysis (cOMP and  
302 eOMP) to the water samples with pressure  $\geq 50$  dbar, to avoid the non-conservative behaviour of  $\theta$   
303 and S in the surface layer due to air–sea interactions after the last maximum of winter convection.  
304 Additionally, we included special SWTs for the regions of intense air–sea interactions (section  
305 2.2.1). We also avoided the input of high percentages of fresh water over the Greenland shelf by  
306 restricting the analysis in this region to water samples with  $S > 34.7$  (Daniault et al., 2011).

307 Some of the SWTs were geographically constrained (Álvarez et al., 2004) according to the  
308 spreading of the water masses: MW was restricted south of the NAC front; DSOW and IrSPMW  
309 were restricted to the Irminger Basin; PIW was restricted to stations over the Greenland slope (in  
310 mixing *figure* 1; Fig. 3c) since it is part of the East Greenland Current (Pickart et al., 2005), and  
311 within the DSOW mixing *figure* (in mixing *figure* 3) since it is assumed to contribute to DSOW  
312 (Falina et al., 2012); and LSW was not allowed in the East Greenland Current (Falina et al., 2012;  
313 von Appen et al., 2014).

314 To reduce the error of the whole OMP analysis, an iterative process was performed for  
315 nutrients (Álvarez et al., 2004), since they accumulate the highest errors (section A1 of the  
316 Appendix). At each iteration we obtained new values of the nutrients for each SWT from  $X_i$ s and  
317 the measured data (eOMP equations). These new estimated values were assigned to the SWTs  
318 and the methodology was re-run. The process finishes when an asymptote is found in the value of  
319 the total residual of the analysis (eOMP) (in this work five iterations were performed). The iterative  
320 process improves the definition of the SWTs, thereby also improving the accuracy of the  
321 methodology.

322 We tested the robustness of the methodology through a perturbation analysis (Lawson and  
323 Hanson, 1974), where the physicochemical properties of each SWT (Álvarez et al., 2004; Pardo et  
324 al., 2012) and of each water sample (Álvarez et al., 2014) were modified by introducing normally  
325 distributed random numbers (section A2 of the Appendix). The resulting uncertainties in the  $X_i$ s  
326 range were between 0.015 and 0.13 (Table 2), indicating that the methodology is robust.

327 Additionally, our model is consistent since its residuals lack a tendency with depth (section A3 of  
328 the Appendix) and the Standard Deviations of the Residuals remain low, slightly higher than the  
329 corresponding measurement error (Table 2). Besides, the model's ability to reproduce the  
330 measured values is given as the correlation coefficient ( $r^2$ ) between the measured (water samples)  
331 and the expected values for the SWTs properties (values of the properties of each water sample  
332 obtained by substituting  $X_i$ s in the system of equations; section A1 of the Appendix). The  $r^2$  values  
333 are higher than 0.94, indicating again the reliability of our methodology.

334 When evaluating the water mass distributions derived from an OMP analysis, it should be  
335 taken into account that the properties that define the SWTs are time invariant; hence, changes in  
336 the properties of the water masses over time are reflected through water mass redistributions.  
337 Therefore, it is possible that some of the changes in the distribution of the SWTs may actually  
338 reflect inter-annual variations in the water mass properties not taken into account in the OMP set-  
339 up, and not only an increase/reduction of its extension. This affects water masses such as LSW  
340 and SPMW, whose properties vary from year to year due to formation processes and air-sea  
341 interaction differences.

### 342 **2.3. Velocity field**

343 The velocity fields in the sections are required to compute the volume transports by water  
344 mass. The velocity fields were obtained from the results of previous studies realized over the same  
345 sections using linear box inverse models. The inverse model configurations for 4x and OVIDE  
346 2002 have been described by Lherminier et al. (2007), for OVIDE 2004 by Lherminier et al. (2010),  
347 for OVIDE 2006 by Gourcuff et al. (2011), and for OVIDE 2008 and 2010 by Mercier et al. (2015).

348 The inverse model is based on the least-squares formalism, which provides errors on the  
349 velocities and associated quantities such as the magnitude of AMOC (estimated in density  
350 coordinate) and the heat flux (Lherminier et al., 2010). The inverse model was constrained by  
351 direct Acoustic Doppler Current Profiler velocity measurements and by an overall mass balance of  
352  $1 \pm 3$  Sv to the North (Lherminier et al., 2007, 2010).

353 The inverse model computes the absolute geostrophic transports orthogonal to the section.  
354 The Ekman transport is deduced from the wind fields averaged over the cruise period and added  
355 homogeneously in the first 40 metres (Mercier et al., 2015). The transport estimates of the inverse  
356 model across OVIDE have been validated by favourable comparisons with independent  
357 measurements (Gourcuff et al., 2011; Danialt et al., 2011; Mercier et al., 2015).

#### 358 **2.4. Combining the water mass distributions with the velocity fields**

359 The combination of the  $X_i$ s ( $i = 1$  to 14) obtained using the OMP analysis with the velocity  
360 fields allowed us to obtain the volume transport of each SWT in the whole water column (Álvarez et  
361 al., 2004).

362 The  $X_i$ s were obtained at each measured point (i.e., bottle depth) for each hydrographic  
363 station, whereas the geostrophic and Ekman components of the flow were estimated at mid-  
364 distance between two hydrographic stations (defining a station pair) with a vertical resolution of 1  
365 dbar. To match the velocity field, the SWT distributions were linearly interpolated at each dbar, and  
366 averaged in station pairs. The velocity field was obtained from the CTD downcast and the  
367 biogeochemical measurements (leading to the  $X_i$ s) were performed during the CTD upcast. To  
368 better match up both fields and compensate for vertical displacements of the water masses  
369 between the CTD downcast and upcast, we used density coordinates instead of pressure  
370 coordinates to interpolate the  $X_i$ s. To obtain  $X_i$ s until the bottom depth of each station pair, the  
371 shallower station profile in each station pair was extended until the maximum depth of the station  
372 pair by copying down the  $X_i$  values of the deepest measured point available.

373 Data of the upper layer (pressure  $\leq 50$  dbar) and of the Greenland shelf waters with  $S <$   
374  $34.7$ , excluded from the OMP analysis, were appropriately reconstructed. The shallowest mixing  
375 contributions at each station of the upper layer were extrapolated up to the surface by keeping the  
376 same  $X_i$  values. In areas close to the Greenland shelf, water samples with  $S < 34.7$  were  
377 substituted by the nearest water sample included in the analysis.

### 378 **3. Water mass distributions for the first decade of the 2000s**

379 The water mass distributions were obtained for each repeat of the OVIDE section by means  
380 of an OMP analysis (section 2.2). It is important to remember that the water mass distributions  
381 presented in this study should be regarded as a best estimate and serve to illustrate the relative  
382 importance of the water masses, since the definitions of the SWTs in the OMP analysis mostly  
383 condition the distribution and the maximum contribution achieved by each SWT. Additionally, we  
384 have to point out that NEADW<sub>U</sub> is not shown because it was considered as a composite SWT  
385 (Álvarez et al., 2004; Carracedo et al., 2012) that can be derived from the mixing of 1.5 % of MW,  
386 18.4 % of LSW, 29.5 % of ISOW and 50.5 % of NEADW<sub>L</sub> (decomposition based on  $\theta$ , S and SiO<sub>2</sub>  
387 content in the different water masses and on the work of van Aken (2000)). In this section, we  
388 describe and discuss the relevant features of the distributions of each SWT for the mean result of  
389 the OVIDE period (2002–2010) (Fig. 4).

### 390 **3.1. Upper waters**

391 The Central Waters (ENACW<sub>16</sub> + ENACW<sub>12</sub>) occupy the upper eastern part of the OVIDE  
392 section from the Iberian Peninsula until the Reykjanes Ridge (Fig. 4a), representing an average of  
393  $14.58 \pm 0.14$  % of the total volume of the five sections. They follow the  $\theta$  maximum and the SiO<sub>2</sub>  
394 minimum over the Iberian Basin (Fig. 2a, e). Their distribution is associated with the circulation of  
395 the NAC, being the  $\theta$ /S front caused by the northern branch of the NAC (located at 25°W in the  
396 OVIDE sections, Fig. 2a, b) the western limit of the Central Waters distribution. The Central Waters  
397 main core extends westwards, reflecting the cyclonic circulation of the Central Waters in the  
398 Iceland Basin and their southward flow over the eastern flank of the Reykjanes Ridge (Read, 2000;  
399 Pollard et al., 2004).

400 The main core of IcSPMW (SPMW<sub>8</sub> + SPMW<sub>7</sub>) is over the Reykjanes Ridge (Fig. 4c).  
401 IcSPMW reaches the surface in the Irminger Basin, although it is formed in the Iceland Basin by  
402 the transformation (air–sea interactions) of the Central Waters (Thierry et al., 2008). This indicates  
403 that, at the time of OVIDE sections (summer), the surface waters in the Iceland Basin were warmer  
404 than 8°C. Furthermore, SAIW is also present in the surface waters of this basin, where it mixes  
405 with IcSPMW and the Central Waters. The distribution of IcSPMW also shows the transport of

406 SPMW from the Iceland Basin to the Irminger Basin by the NAC (Irminger Current) (Brambilla and  
407 Talley, 2008).

408 IrSPMW extends from the Greenland slope until the Reykjanes Ridge (Fig. 4d), with its  
409 main core over the Greenland slope. This distribution could indicate that the major region of  
410 formation of IrSPMW could be the NW of the Irminger Basin (Brambilla and Talley, 2008), from  
411 where the East Greenland Irminger Current would transport it until the OVIDE section. This SWT  
412 can be treated as a precursor of the upper LSW (Pickart et al., 2003). The continuity of the  
413 distributions of the Central Waters, IcSPMW and IrSPMW indicates that IrSPMW is the final  
414 product of the transformation of the Central Waters due to air–sea interaction processes  
415 (McCartney and Talley, 1982; Brambilla and Talley, 2008), IcSPMW being the intermediate point of  
416 the transformation.

### 417 **3.2. Intermediate waters**

418 SAIW (SAIW<sub>6</sub> + SAIW<sub>4</sub>) is present in the upper layers of the northern half of the OVIDE  
419 sections (Fig. 4b). The distribution of SAIW shows a maximum in the Iceland Basin associated with  
420 its advection from the Labrador Sea within the NAC and its subduction beneath the Central Waters  
421 (Bubnov, 1968; Arhan, 1990; Read, 2000). SAIW suffers a sharp decline once it encounters the  
422 NAC, but its contribution is significant until 600 m depth, where it still represents percentages  
423 greater than 25 %. East of the Rockall Bank (Fig. 1), SAIW deepens until intermediate water  
424 depths, where it overlies MW (Pollard et al., 1996). In fact, SAIW and MW contribute together to  
425 their surrounding waters in the region southeast of the NAC (Figs. 1 and 4b, d) (Harvey and Arhan,  
426 1988).

427 The main core of MW is located around 1200 m depth off the shelf of the Iberian Basin (Fig.  
428 4d, see the tongue of maximum S and minimum O<sub>2</sub> in Fig. 2b, c), with a maximum of  $83.4 \pm 0.9$  %  
429 coinciding with the S maximum of  $36.28 \pm 0.01$  (n = 5; where n is the number of cruises). This main  
430 core is associated with the northward flow of MW (Reid, 1979) and extends westwards, which  
431 could be associated with its transport by meddies (Mazé et al., 1997) and by the Azores  
432 countercurrent (Carracedo et al., 2014).

433 LSW is the dominant SWT in the sections ( $35.0 \pm 0.6$  % of the section volume,  $n = 5$ ; Fig.  
434 4e). It mainly extends from 1000 to 2500 m depth, coinciding with the S minimum ( $34.91 \pm 0.02$ )  
435 and a relative  $O_2$  maximum ( $285 \pm 2 \mu\text{mol kg}^{-1}$ ) found in all the three basins (Fig. 2b, c). LSW  
436 presents two main cores separated by the Reykjanes Ridge, which correspond to the different  
437 pathways of its circulation (Pickart et al., 2003; Álvarez et al., 2004). This “gap” separating the two  
438 LSW cores suggests a relatively strong mixing around and over the Reykjanes Ridge (Ferron et al.,  
439 2014), where the presence of fractions greater than 20 % of ISOW and IcSPMW induces a  
440 decrease in LSW. This erosion of the LSW core is also reflected by a reduction of the S minimum  
441 over the Reykjanes Ridge (Fig. 2b). Moreover, this is the location of the water mass described as  
442 the Icelandic Slope Water by Yashayaev et al. (2007), which is defined as a result of the direct  
443 mixing of ISOW with Atlantic waters, mixing represented in our work by the mixing *figure 4* (Fig.  
444 3c). In agreement with the work of Read (2000), the depth of the LSW core in the Irminger Basin is  
445 shallower than the one spreading across the Iceland and Iberian Basins, although they stay at the  
446 same density (see isopycnal  $\sigma_1 = 32.42$ , dashed line on Fig. 4e; where  $\sigma_1$  is potential density  
447 referenced to 1000 dbar). The contribution of LSW in the south-eastern part of the sections is high  
448 (reaching maximum values of  $76 \pm 1$  %,  $n = 5$ ), emphasizing the influence of LSW until areas close  
449 to the Iberian Peninsula (Tsuchiya et al., 1992; Arhan et al., 1994; Paillet et al., 1998). Moreover,  
450 the volume occupied by LSW gradually decreases from the Irminger Basin to the Iberian Basin. It  
451 represents  $45 \pm 1$  % ( $n = 5$ ) of the volume of the Irminger Basin (defined between the Greenland  
452 slope and the Reykjanes Ridge),  $45 \pm 1$  % of the volume of the Iceland Basin (defined from the  
453 Reykjanes Ridge until  $25.5^\circ\text{W}$ ) and  $30.3 \pm 0.5$  % of the volume of the Iberian Basin (note that the  
454 volumes of the basins refer to the volumes at the section location, and the volumes per water mass  
455 are computed by weighting the volume of the basin by the SWT contribution).

### 456 **3.3. Overflows and deep waters**

457 ISOW comes from the Iceland–Scotland sills and flows southwards along the eastern flank  
458 of the Reykjanes Ridge, where its main core is found (Fig. 4b). This main core is located at depths  
459 greater than 2300 m, with maximum percentages of  $90 \pm 2$  % ( $n = 5$ ), where the  $\theta/S$  properties are

460  $2.59 \pm 0.03^{\circ}\text{C}$  and  $34.979 \pm 0.002$ , respectively. From this region the core extends eastwards  
461 between  $\sim 2000$  and  $4000$  m depth, reaching values of 10 % in the Iberian Abyssal Plain (Fig. 1).  
462 This eastward extension could reveal that some ISOW must bypass the CGFZ and flow into the  
463 West European Basin. This feature is captured by the OMP analysis, since it is capable of  
464 capturing the significant fractions of the water masses better than the classical water mass  
465 descriptions. ISOW is also detected at the bottom in the central and eastern regions of the Irminger  
466 Basin, associated with its northward spreading after crossing the CGFZ (Dickson and Brown, 1994;  
467 Saunders, 2001). These findings could also be related to the northward flow of ISOW mainly in the  
468 interior part of the Irminger Basin (Sarafanov et al., 2012).

469 The deepest part of the Greenland continental slope is occupied by DSOW (Fig. 4a). The  
470 distribution of this water mass can be traced in the vertical sections of the OVIDE mean properties  
471 (Fig. 2) as a minimum of  $\theta$  ( $< 2^{\circ}\text{C}$ ), a maximum of  $\text{O}_2$  ( $> 280 \mu\text{mol kg}^{-1}$ ) and a relative minimum of  
472 nutrients. The inclusion of PIW in the analysis is an attempt to model the entrainment of shelf  
473 waters into the deep waters of the Irminger Basin (Tanhua et al., 2008; Falina et al., 2012; von  
474 Appen et al., 2014). The presence of PIW (Fig. 4f), even though in a very narrow area, supports  
475 the statement of the existence of certain dynamical processes that link the East Greenland shelf  
476 waters with the deep overflows.

477 NEADW<sub>L</sub> is the dominant water mass in the Iberian Basin from 2000 m depth to the bottom,  
478 with the main core below  $\sim 3500$  m depth (Fig. 4f). The distribution of this water mass follows the  
479 high  $\text{SiO}_2$  concentrations at the bottom of the Iberian Basin ( $> 20 \mu\text{mol kg}^{-1}$ ; Fig. 2e), which are  
480 coupled with high concentrations of  $\text{NO}_3$  and  $\text{PO}_4$  (Fig. 2d, f, respectively). The high  $\text{SiO}_2$  levels  
481 reflect the influence of Antarctic Bottom Water (van Aken and Becker, 1996). The NEADW<sub>L</sub>  
482 isolines shallow eastwards due to the general deep eastern boundary upwelling of this water mass  
483 along the coast of the Iberian Peninsula (Arhan et al., 1994). The northern part of the distribution of  
484 NEADW<sub>L</sub> is affected by the influences of LSW and ISOW.

#### 485 **4. Time variability of the water mass distributions between 1997 and 2010**

486 In this section, we select SPMW (IcSPMW + IrSPMW), LSW and the deep overflows  
487 (DSOW and ISOW) to describe and discuss their variability from 1997 to 2010 (Fig. 5). It should be  
488 mentioned that the different section pathways (Fig. 1) could generate differences in the SWT  
489 distribution patterns between the 4x and OVIDE sections. The overlapping of the METEOR and  
490 OVIDE sections allows us to distinguish between the differences in the SWTs distributions due to  
491 the different section pathways, and the inter-annual variability.

492 From the comparison of the LSW distributions in both cruises of 1997, we can conclude that  
493 for the Irminger Basin the difference in the section pathway between the 4x and OVIDE sections is  
494 negligible, whereas for the Iceland Basin and around the Reykjanes Ridge it is an important  
495 component of the variability of the LSW distributions (Fig. 5). In the Irminger Basin, from 1997 to  
496 2010 the contribution of LSW gradually decreases, which is in agreement with the almost complete  
497 disappearance of the LSW signal found in 2007 by de Jong et al. (2012). LSW represents 58 % of  
498 the volume of the Irminger Basin in 1997, then its importance decreases over time, representing 50  
499 % for 2002, with a sharp decrease in 2006 when it drops to 43 %, a percentage that remains until  
500 2010. The LSW maximum in the Iceland Basin decreases more slowly than the one in the Irminger  
501 Basin, meaning that in 2004 the fractions of the core in the Iceland Basin are higher (> 95 %) than  
502 those of the core in the Irminger Basin (< 90 %). This contrast is most noticeable in 2006 due to  
503 the sharp decrease in the fractions of LSW in the Irminger Basin. In the West European Basin (Fig.  
504 1) the greatest change in the fractions of LSW takes place in 2008, when the extension of the core  
505 is reduced in both the Iceland and the West European Basins, a reduction that continues in 2010.  
506 However, the volume occupied by LSW in the Iberian Basin is almost constant over time ( $30.3 \pm$   
507  $0.5$  % for the period 2002–2010), which indicates that the large inter-annual variability of the  
508 properties in its formation region attenuates due to mixing over the length and timescales of the  
509 transit from the Labrador Sea (Cunningham and Haine, 1995; Paillet et al., 1998). The difference in  
510 years between the deepening and total extension of LSW could be related to the changes in the  
511 volume of LSW formed. Between 1987 and 1995 the change in the NAO index led to the  
512 diminution in volume and also the warming and salinization of LSW over time (Lazier et al., 2002;  
513 Yashayaev, 2007). These changes in the LSW properties are solved by the OMP analysis by  
514 adding more SPMW.

515 The SPMW (IcSPMW + IrSPMW) distribution presents the greatest change between the  
516 two sections carried out in 1997 (Fig. 5), which indicates that the section pathway influences the  
517 SPMW distribution since both cruises took place in the same time frame. The main path of the  
518 NAC around the Reykjanes Ridge is located north of the 4x section location (Fig. 1) so that the  
519 fractions of SPMW observed at the 4x location are lower than at the OVIDE location. Meanwhile,  
520 the METEOR section presents an SPMW distribution similar to those of the OVIDE sections.  
521 Between 1997 (METEOR) and 2010, the importance of SPMW increases, rising from 24 % to 30 %  
522 of the volume of the Irminger Basin, with a rate of increase of 0.5 % per year ( $r^2 = 0.93$ ), driven  
523 mainly by the increase in the upper 1000 m over the Reykjanes Ridge (0.7 % per year,  $r^2 = 0.95$ ).  
524 This change may be related to the difference in the properties of the water masses at their  
525 formation regions. Since the end of the 1990s, the upper-ocean and upper intermediate waters of  
526 the NASPG have been getting saltier and warmer due to the redistribution of subpolar and  
527 subtropical waters caused by the NAO-induced slowdown and contraction of the NASPG (Bersch,  
528 2002; Hátún et al., 2005; Sarafanov, 2009; de Boisséson et al., 2012). Thus, the 1997 section  
529 presents fresher waters than the 2000s sections, and the OMP replaces there less SPMW and  
530 more LSW. Moreover, the increasing amount of SPMW in the centre of the Irminger Basin could be  
531 associated with the reduction of the deep convection in the Labrador Sea, which resulted in a  
532 shallower variety of LSW (Pickart et al., 1996; Stramma et al., 2004; Bersch et al., 2007). The  
533 thickening observed in the SPMW distributions could indicate a salinization of LSW, solved by the  
534 OMP by adding greater fractions of SPMW.

535 The inter-annual variability of the depth, location and importance of LSW and SPMW seems  
536 to be connected. These results are in agreement with the interplay that exists between these water  
537 masses (Bersch et al., 1999). The upper parts of the Irminger Basin gain SPMW and lose LSW  
538 over time, demonstrating the ability of our OMP methodology to capture the different vintages of  
539 LSW formed over time (Yashayaev et al., 2008).

540 The distribution of ISOW is also influenced by the section pathway that is reflected by the  
541 differences in its distribution between the two 1997 cruises. For the 4x section the percentages of  
542 the ISOW core located over the eastern flank of the Reykjanes Ridge fall below 70 %, whereas for  
543 the METEOR section it reaches percentages greater than 80 % (Fig. 5). This difference could be

544 explained by the flow of part of ISOW through gaps in the Reykjanes Ridge located north of the  
545 CGFZ, between the METEOR and 4x sections, as found by Xu et al. (2010). The existence of  
546 various deep passages between the locations of the sections (Fig. 1) may reduce the arrival of  
547 ISOW to the 4x section. The distribution of ISOW in the Irminger Basin also differs between the 4x  
548 and METEOR sections. The 4x section is located just after the CGFZ, so that the ISOW  
549 distributions on both sides of the ridge are similar. Meanwhile, in the METEOR section, the great  
550 distance between the fracture zone and the section causes ISOW to arrive more diluted at the  
551 section location after flowing anticyclonically around the ridge. For the same section pathway  
552 (METEOR-OVIDE), we found slight inter-annual changes in the distributions of ISOW on both  
553 sides of the Reykjanes Ridge. The core over the eastern flank of the ridge expands and contracts  
554 between cruises, which could reflect the inter-annual variability of the properties and sources of  
555 ISOW (Sarafanov et al., 2010). For the Irminger Basin, the ISOW influence increases over time,  
556 with the greatest change between 1997 (2 % of volume) and 2002 (10 %), increasing in importance  
557 until 2010 (15 %), although with some inter-annual variability. The great difference between the  
558 ISOW distributions of the Irminger Basin in 1997 (METEOR) and 2002 could be related to the  
559 different LSW distribution on the two cruises. In 1997, after a period of high NAO index when large  
560 amounts of LSW were formed (Lazier et al., 2002; Yashayaev, 2007), LSW occupied almost the  
561 whole Irminger Basin, leaving little space for ISOW. In 2002, the reduction of the percentages of  
562 LSW allowed more ISOW to enter the Irminger Basin. These results are also supported by the  
563 increase of S in the Irminger Basin in the density range of ISOW found by Sarafanov et al. (2010).  
564 Since the properties that define an SWT are time invariant, the OMP analysis solves this increase  
565 of S by giving more presence to ISOW and less to LSW. This is also consistent with the increase of  
566 S in LSW (Lazier et al., 2002; Pickart et al., 2003; Kieke et al., 2007).

567 For 1997, DSOW seems to be colder at the 4x location than at the OVIDE location, which is  
568 reflected by lower percentages of DSOW and higher of PIW (Fig. 5). This could indicate that (i) at  
569 4x location the spill jet, represented by PIW, is not completely mixed with DSOW and the two  
570 SWTs can be more easily distinguished; and (ii) the existence of strong mixing between the two  
571 section locations led to a well-defined DSOW at the OVIDE location. Between METEOR and 2010,  
572 the DSOW distributions present no apparent trend at inter-annual timescales. In 2002 and 2004

573 the PIW influence in the DSOW layer is greater than in the other years, which is in agreement with  
574 the entrainment events observed by Falina et al. (2012). Adding the PIW contributions of mixing  
575 *figure 3* (Fig. 3c) to those of DSOW, we can observe this increase in the overflow volume. In both  
576 years, the DSOW contributions are greater, reaching more than 5.0 % of the volume of the  
577 Irminger Basin, while in the other cruises its percentages do not exceed 4.5 %. Probably, these  
578 changes could be associated with inter-annual variability in the water sources and transports of the  
579 overflows (Falina et al., 2012), which could ultimately be related to changes in the atmospheric  
580 forcing (Macrander et al., 2005), but we lack sufficient data to relate these changes to a given  
581 timescale.

## 582 **5. Water mass volume transports, recirculation and transformations in the Subpolar North** 583 **Atlantic**

584 For each OVIDE cruise the  $X_i$ s were combined with the absolute geostrophic velocity field  
585 (section 2.4) to obtain the water mass volume transports. Then we computed the mean water mass  
586 volume transports for the period 2002–2010 and integrated them along the section to obtain the  
587 net water mass volume transports (represented in Sverdrup;  $1 \text{ Sv} = 10^6 \text{ m}^3 \text{ s}^{-1}$ ) (Fig. 6). The water  
588 mass volume transports were calculated perpendicular to the sections and are positive northwards.  
589 Errors were computed by weighting the velocity errors by the  $X_i$ s. The velocity errors were  
590 computed at the reference level using the error covariance matrix of the inversion (Mercier, 1986;  
591 Lherminier et al., 2007, 2010). It is important to note that the water mass volume transport  
592 estimates are sensitive to the distribution of the SWTs.

593 The water masses that contribute to the northward transport in the section are the Central  
594 Waters ( $11.6 \pm 1.2 \text{ Sv}$ ), IcSPMW ( $2.6 \pm 1.5 \text{ Sv}$ ), SAIW ( $2.2 \pm 0.4 \text{ Sv}$ ) and MW ( $0.2 \pm 0.4 \text{ Sv}$ ) (Fig.  
595 6). These are the first estimates of the transports of the Central Waters, SPMW and SAIW in the  
596 Subpolar North Atlantic apart from the transports of the Central Waters and SAIW reported for the  
597 4x section by Álvarez et al. (2004) (10.3 and 2.9 Sv, respectively). Our MW transport is lower than  
598 that reported by Álvarez et al. (2004) and Schmitz (1996). This may be due to the variability  
599 derived from its transport by meddies (Arhan and King, 1995; Mazé et al., 1997).

600 The transformation of the above-cited water masses leads to the formation of IrSPMW,  
601 which transport ( $-8.8 \pm 0.9$  Sv; Fig. 6) is concentrated in the East Greenland Irminger Current. This  
602 water mass represents an important fraction of the  $-22.1 \pm 3.2$  Sv of the East Greenland Irminger  
603 Current estimated for the OVIDE sections of 2002 and 2004 by Lherminier et al. (2010). IrSPMW is  
604 the precursor of LSW, whose net transport across the OVIDE section is southwards ( $-0.9 \pm 1.8$  Sv).  
605 This net southward transport of LSW, in agreement with a moderate formation of LSW in the  
606 Irminger Basin (Pickart et al., 2003), is explained by the strong southward transports found in the  
607 East Greenland Irminger Current, where small amounts of LSW lead to great southward transports.  
608 Lherminier et al. (2007) reported a net northward export of LSW in the OVIDE section, while Bacon  
609 (1997) found a net transport of  $-1$  Sv of LSW in a section close to the OVIDE section. The most  
610 likely explanation for the difference between our results and the two previous ones could lie in the  
611 specificities of the distributions obtained from the OMP analysis. The SWTs distributions are not  
612 defined by isopycnal ranges but as dilution from a “pure” SWT, so the OMP methodology assesses  
613 all the water mass contributions, even those outside the core of the water mass. This feature  
614 together with the inter-relation between LSW, SPMW and ISOW in the Irminger Basin (sections 3  
615 and 4) could result in this kind of difference in the transport estimates.

616 The water masses coming from the sills are PIW, DSOW and ISOW. The PIW transports  
617 were split into two main cores: a shallow one associated with mixing *figure 1*, and a deep one  
618 associated with mixing *figure 3* (Fig. 3c; section 2.2.2). For the shallow core of PIW the net  
619 transport is  $-1.3 \pm 0.1$  Sv (Fig. 6). This transport is slightly lower than those reported by Pickart et  
620 al. (2005) (barely  $-2$  Sv) and Falina et al. (2012) ( $-2.4 \pm 0.3$  Sv as mean transport for 2002–2004).  
621 This could be because the transports associated with the deep core of PIW were added to those of  
622 DSOW. Nevertheless, it is in agreement with the  $-1.3$  Sv of upper waters estimated to enter the  
623 Irminger Basin from the Nordic Seas (Hansen and Österhus, 2000). The transport of DSOW across  
624 the OVIDE section is  $-2.5 \pm 0.3$  Sv, which is in good agreement with the estimates of Ross (1984)  
625 (from  $-2$  to  $-3$  Sv), Eden and Willebrand (2001) ( $-2.5$  Sv), and Lherminier et al. (2010) ( $-2$  Sv, for  
626 the OVIDE sections of 2002 and 2004). However, our estimate is slightly lower than the  $-3$  Sv  
627 found by Dickson and Brown (1994), the  $-3.5 \pm 1.6$  Sv found by Macrander et al. (2005) and the  
628  $-3.4 \pm 1.4$  Sv found by Jochumsen et al. (2012). Since in this study the assessment of the water

629 mass volume transports is based on dilutions of a “pure” SWT, it would be expected to have lower  
630 volume transports than those estimated by isopycnals. These underestimates are compensated by  
631 the mixing with other SWTs (ISOW and LSW). The net transport of ISOW is  $-2.7 \pm 0.8$  Sv, a result  
632 supported by the  $-3.2 \pm 0.5$  Sv reported by Saunders (1996), the  $-3.6 \pm 0.5$  Sv reported by van  
633 Aken and Becker (1996), the  $-2.5 \pm 0.9$  Sv reported by Lherminier et al. (2007) and the  $-3.7 \pm 0.8$   
634 Sv reported by Sarafanov et al. (2012). Finally, NEADW<sub>L</sub> also contributes to the net pull of the  
635 deep waters in the NASPG. The net transport of this water mass ( $0.6 \pm 1.2$  Sv) is comparable with  
636 the 1.1 Sv reported by van Aken and Becker (1996).

637 In a recent study, Mercier et al. (2015) estimated the magnitude of the upper and lower  
638 limbs of the AMOC (in density coordinates) for the OVIDE sections. These authors reported a  
639 magnitude of the upper limb of the AMOC of  $16.2 \pm 2.4$  Sv; and of  $-15.5 \pm 2.4$  Sv for the AMOC  
640 lower limb for the OVIDE period (2002–2010). Considering the isopycnal that separates the upper  
641 and lower limbs in Mercier et al. (2015) ( $\sigma_1 = 32.15$ ), the upper limb of the AMOC in our study is  
642 represented by the Central Waters, IcSPMW and SAIW. We also included the net northward  
643 transport of MW (Fig. 6) in the AMOC upper limb. These flows altogether result in an AMOC upper  
644 limb of  $16.6 \pm 1.5$  Sv for the OVIDE period. These upper AMOC contributors resemble the  
645 subtropical (Central Waters) and subpolar (SAIW and IcSPMW) components of the AMOC at the  
646 OVIDE sections described by Desbruyères et al. (2013). The lower limb of the AMOC is constituted  
647 by IrSPMW, PIW, LSW, ISOW, DSOW and NEADW<sub>L</sub>, resulting in a southward transport of  $-15.6 \pm$   
648  $2.5$  Sv. Although in our study the water masses that contribute to the upper and lower limbs of the  
649 AMOC may overlap both limbs, our approach is in good agreement with the findings of Mercier et  
650 al. (2015). Combining the  $X_i$ s of the 4x section, obtained using the OMP methodology, with the  
651 velocity field of the section (Lherminier et al., 2007), we reevaluated the water mass volume  
652 transports of the 4x section reported by Álvarez et al. (2004). For this section, the magnitudes of  
653 the upper and lower limbs of the AMOC obtained from the water masses contributing to each limb  
654 are  $23.3 \pm 1.2$  Sv and  $-21.1 \pm 1.8$  Sv, respectively. The difference with respect to the magnitude of  
655 the AMOC for the OVIDE period is explained by the greater transports in 1997 of the Central  
656 Waters ( $17.4 \pm 1.2$  Sv), IrSPMW ( $-12.0 \pm 0.3$  Sv) and PIW ( $-3.1 \pm 0.1$  Sv). Our results support the  
657 findings of Mercier et al. (2015), who concluded that the decrease in the northward subsurface

658 transport of the AMOC from 1993 to 2010 was balanced, at least partially, by a decrease in the  
659 southward export of the intermediate waters in the western Irminger Basin. These changes could  
660 be linked to a change in the circulation in response to a transition from previously high to low NAO  
661 indices over this time span (1997–2000s).

662 Taking advantage of the estimated water mass volume transports, we also inferred the  
663 water mass circulation and transformation in the Subpolar North Atlantic based on four boxes  
664 defined following Lherminier et al. (2010) and limited to the south by the OVIDE section and to the  
665 north by the Greenland–Iceland–Scotland sills (Fig. 7). The region east of the Reykjanes Ridge will  
666 be referred to as the East North Atlantic (ENA) Basin and the region west of the Reykjanes Ridge  
667 as the Irminger Basin. The final four boxes were obtained by dividing both basins vertically by the  
668 isopycnal  $\sigma_2 = 36.94$ , which traditionally defines the upper bound of the deep waters. Considering  
669 that no passages deeper than this isopycnal exist in the ridge between Iceland and the OVIDE  
670 section, this isopycnal also separates the water masses that can cross the Reykjanes Ridge (upper  
671 boxes) from those that cannot (lower boxes), which sets an additional constraint on the volume  
672 budgets. The water mass volume transports are considered positive when entering the boxes.

673 In order to obtain the volume budgets of the boxes, we considered the volume transports  
674 estimates through the Greenland–Iceland–Scotland sills available in the literature (Fig. 7, grey  
675 numbers). In the ENA Basin, -7 Sv of relatively warm water ( $> 7^\circ\text{C}$ ) flow north-eastwards past the  
676 Faroes (Fig. 1) (Schmitz and McCartney, 1993; van Aken and Becker, 1996; Hansen and  
677 Österhus, 2000), while 3 Sv enter the basin via the overflow waters (Olsen et al., 2008). In the  
678 Irminger Basin, 1.3 Sv of upper waters (Hansen and Österhus, 2000) and 3 Sv of overflow waters  
679 (Olsen et al., 2008) enter this basin from the Nordic Seas, whereas -1 Sv of Atlantic water exits this  
680 basin towards the Nordic Seas (Hansen and Österhus, 2000). The volume transports at the  
681 southern limit of the boxes (OVIDE section) are the mean volume transports across the OVIDE  
682 sections (section 3).

683 The net volume transport in the ENA Basin across the OVIDE section is  $13.4 \pm 4.7$  Sv and  
684 across the Iceland–Scotland sills is -4 Sv (Fig. 7a, c). As a result,  $9.4 \pm 4.7$  Sv should flow from the  
685 ENA Basin to the Irminger Basin over the Reykjanes Ridge. This is corroborated by the volume  
686 budget of the Irminger Basin, where the difference between the net volume transport across the

687 OVIDE section ( $-12.6 \pm 4.7$  Sv) and that across the Greenland–Scotland sills ( $3.3$  Sv) is  $-9.5 \pm 4.7$   
688 Sv. These estimates are very similar to the  $11.7 \pm 2.1$  Sv estimated by Lherminier et al. (2010) for  
689 the mean of the 2002–2004 OVIDE sections and to the  $9.1 \pm 1.8$  Sv estimated by Sarafanov et al.  
690 (2012) for the region between  $59.5^\circ\text{N}$  and the Greenland–Iceland–Scotland sills.

691 Of the  $3$  Sv of overflow waters entering the lower ENA box, only  $-1.3 \pm 2.6$  Sv exit this box  
692 across the OVIDE section (Fig. 7c). This implies that  $1.7 \pm 2.6$  Sv should upwell and become part  
693 of the upper ENA box. In fact, these  $1.7 \pm 3.9$  Sv are necessary in the upper ENA box to balance  
694 the volume transports (Fig. 7a). For the upper Irminger box,  $0.3$  Sv enter via the Greenland–  
695 Iceland sills and  $9.4 \pm 4.7$  Sv enter over the Reykjanes Ridge. Only  $-6.2 \pm 4.2$  Sv exit the box  
696 across the OVIDE section, thus implying that  $3.5 \pm 6.3$  Sv should sink and become part of the  
697 lower Irminger box. In this lower Irminger box,  $3$  Sv enter via the overflow waters and  $-6.4 \pm 2.2$  Sv  
698 exit across the OVIDE section, thereby  $3.4 \pm 2.2$  Sv are missing, and would be those from the  
699 upper Irminger box (Fig. 7c). This is in agreement with the mean results for the 2002–2004 OVIDE  
700 sections of Lherminier et al. (2010), who estimated that  $3.9 \pm 1.8$  Sv cross from the upper to the  
701 lower box of the Irminger Basin.

702 The OMP-based water mass distributions let us disaggregate the water masses that are  
703 involved in each of those volume transports. The  $1.7 \pm 2.6$  Sv upwelling from the lower to the upper  
704 ENA box should be ISOW, since from the  $3$  Sv of overflow waters entering the lower ENA box, only  
705  $-1.4 \pm 1.0$  Sv leave the box across the OVIDE section. Thus, the remaining  $1.6 \pm 1.0$  Sv should  
706 upwell to the upper ENA box, which is proved by the net southward transport of  $-0.7 \pm 0.2$  Sv of  
707 ISOW in the upper ENA box across the OVIDE section (Fig. 7b). The remaining  $0.9 \pm 0.9$  Sv  
708 should cross over the Reykjanes Ridge, which is consistent with the net southward export of  $-0.6 \pm$   
709  $0.9$  Sv of ISOW in the Irminger Basin across the OVIDE section.

710 In order to estimate the other water mass components of the  $9.4 \pm 4.7$  Sv crossing over the  
711 Reykjanes Ridge, we should first determine the composition of the  $-7$  Sv crossing the Iceland–  
712 Scotland sills northwards. Since this flow has temperatures over  $7^\circ\text{C}$  (Schmitz and McCartney,  
713 1993; van Aken and Becker, 1996), only the Central Waters, IcSPMW and MW (New et al., 2001)  
714 are possible sources. IcSPMW is excluded from this group because it is formed in the Iceland  
715 Basin close to the Reykjanes Ridge (McCartney and Talley, 1982; Tsuchiya et al., 1992; van Aken

716 and Becker, 1996). Considering that the Central Waters and MW account for  $11.8 \pm 1.3$  Sv in the  
717 ENA Basin across the OVIDE section and that  $-7$  Sv cross the Iceland–Scotland sills northwards,  
718  $4.8 \pm 1.3$  Sv are available to flow over the Reykjanes Ridge. MW flows northwards through the  
719 Rockall trough due to mixing with the Central Waters (Pollard et al., 1996; McCartney and  
720 Mauritzen, 2001; New et al., 2001) and does not reach the Reykjanes Ridge, thus the  $4.8 \pm 1.3$  Sv  
721 are attributed to the Central Waters. Once the Central Waters reach the Iceland Basin they  
722 transform into IcSPMW ( $-2.7 \pm 1.3$  Sv), leaving only  $2.1 \pm 1.8$  Sv of Central Waters available for  
723 crossing over the Reykjanes Ridge. The rest of the flow over the ridge corresponds to those waters  
724 colder than  $7^{\circ}\text{C}$  entering the upper ENA box through the OVIDE section, i.e.,  $4.0 \pm 0.5$  Sv of SAIW,  
725  $2.4 \pm 2.0$  Sv of LSW and the  $0.9 \pm 0.9$  Sv of ISOW above estimated. Intensified vertical mixing at  
726 the Reykjanes Ridge (Ferron et al., 2014) could explain the appearance and transports of LSW  
727 and ISOW over the ridge.

728         After crossing the Reykjanes Ridge, LSW and ISOW intrude in the deep-to-bottom levels of  
729 the Irminger Basin, being the main components of the  $3.5$  Sv downwelling from the upper to the  
730 lower Irminger box. In fact, the net flows of LSW and ISOW in the Irminger Basin are almost  
731 compensated by their corresponding flows over the Reykjanes Ridge (Fig. 7b). In the lower  
732 Irminger box, the  $-2.5 \pm 0.3$  Sv of DSOW leaving this box are slightly lower than the  $3$  Sv of  
733 overflow waters entering this box. The deficit in the DSOW volume transport, as explained before,  
734 is compensated by the excess of LSW and ISOW. This disagreement in the volume transports  
735 could be explained by two facts. First, the mixing between IrSPMW and PIW leads to waters with  
736 properties similar to those of LSW, which the OMP analysis assigned as LSW. Second, the  
737 contributions of the spill jet are very difficult to separate from those of LSW (von Appen et al.,  
738 2014), so that part of the spill jet that should be contributing to the DSOW volume transport would  
739 be attributed to the LSW volume transport.

740         In the upper Irminger box, the transport of PIW across the OVIDE section matches the  $1.3$   
741 Sv entering this box from the Nordic Seas. The remaining water masses present in this box  
742 undergo significant transformations. From the  $4.0 \pm 0.5$  Sv of SAIW entering the Irminger Basin  
743 over the Reykjanes Ridge,  $-1.8 \pm 0.3$  Sv exit this basin through the OVIDE section. Besides,  
744 considering that  $-1$  Sv of Atlantic waters leaves the Irminger Basin towards the Nordic Seas,  $3.2 \pm$

745 1.8 Sv of Central Waters and SAIW should have been lost or transformed into other water masses.  
746 Considering that IrSPMW derives from IcSPMW, and that the inputs from the latter only account for  
747  $5.3 \pm 1.2$  Sv in the Irminger Basin (Fig. 7b), the  $3.2 \pm 1.8$  Sv of Central Waters and SAIW should  
748 have contributed to the IrSPMW volume transport. The net southward export of  $-8.8 \pm 0.8$  Sv of  
749 IrSPMW across the OVIDE section is most probably the further precursor of LSW in the Labrador  
750 Sea (Talley and McCartney, 1982).

751 The high variability of the water mass transports around Cape Farewell (Daniault et al.,  
752 2011) hinders a consensus on the estimation of the formation of NADW (Clarke, 1984; Dickson  
753 and Brown, 1994; Bacon, 1997). The classical study of Dickson and Brown (1994) states that  
754 NADW is formed by the merger of ISOW, DSOW, Lower Deep Water (here represented by  
755 NEADW<sub>L</sub>) and minor contributions of LSW. Dickson and Brown (1994) state that the ISOW  
756 transport would increase due to the contribution of the Lower Deep Water and that LSW would  
757 contribute to the increase of the transport of DSOW from the sills until Cape Farewell, which is  
758 corroborated in our study by the net southward transport of LSW in the Irminger lower box (Fig.  
759 7d). If we add the transports of all the contributors of NADW (net transport of DSOW, ISOW and  
760 NEADW<sub>L</sub> across the OVIDE section, and the net transport of LSW in the Irminger lower box across  
761 the OVIDE section), we obtain a production of  $9.0 \pm 0.9$  Sv, a result slightly lower than the  $\sim 10$  Sv  
762 reported by Bacon (1997) at Cape Farewell.

763 Although the water mass volume transports given by the water mass distributions are  
764 sensitive to the distributions of the SWTs, which are subject to the definition of the SWTs, the  
765 volume transports estimated through the water mass distributions are more realistic than those  
766 obtained between density layers. In the studies performed between density layers, the volume  
767 transports between certain isopycnals are assigned entirely to a water mass, while the  
768 methodology described here allows this volume transport to be split between the different water  
769 masses found in this density range, which could lead to water mass volume transports lower than  
770 those estimated through the isopycnal method.

## 771 6. Conclusions

772 In this study we show an application of the OMP analysis to identify temporal variations and  
773 transformations of the water masses along the WOCE A25 hydrographic sections (southern  
774 boundary of the NASPG). Our choice of SWTs and mixing *figures* is appropriate to describe all the  
775 cruise samples, as evidenced by the low residuals of the model. Water mass transformation  
776 through air–sea interactions is taken into account in the OMP set-up by specifying several varieties  
777 of SPMW. This novelty leads to realistic water mass distributions, confirming generally accepted  
778 knowledge of the Subpolar North Atlantic circulation. In particular, our water mass distributions  
779 evidence the subduction of SAIW below the NAC and the PIW cascading to the density of the  
780 Deep Western Boundary Current. We also provide the relative contribution from each water mass  
781 to the transports across the sections by combining the results from the OMP analysis with the  
782 velocity fields of the sections. The assessment of the water mass volume transports based on  
783 dilutions of a “pure” SWT (OMP-based) is particularly useful for areas of complex currents and  
784 relevant processes of water mass transformation, where this combined methodology can provide  
785 robust insights on the circulation features, improving the understanding of the regional  
786 oceanography.

787 The transport estimates by water mass are in good agreement with previous studies and  
788 match the main features of the northern North Atlantic Circulation. Considering the isopycnal that  
789 separates the upper and lower limbs of the AMOC ( $\sigma_1 = 32.15$ ), we associate each SWT with the  
790 corresponding AMOC limb. In our study, the upper limb of the AMOC is represented by the Central  
791 Waters, IcSPMW, SAIW and MW; and the lower limb of the AMOC is constituted by IrSPMW, PIW,  
792 LSW, ISOW, DSOW and NEADW<sub>L</sub>. This allows us to associate the reduction of the magnitude of  
793 the upper limb of the AMOC between 1997 and the 2000s (from  $23.3 \pm 1.2$  Sv to  $16.5 \pm 1.5$  Sv)  
794 with the reduction in the northward transport of the Central Waters. This reduction of the northward  
795 flow of the upper limb of the AMOC is partially compensated by the reduction of the southward flow  
796 of the lower limb of the AMOC, associated with the decrease in the transports of IrSPMW and PIW.

797 The assessment of the box budgets allows us to disentangle the transformation pathway of  
798 the Central Waters. In the ENA Basin, 2.7 Sv of Central Waters are transformed into IcSPMW. This  
799 flow recirculates around the Reykjanes Ridge and joins IcSPMW advected from the south (possibly  
800 through a branch of the NAC as suggested by Pollard et al. (2004)), leading to a northward

801 transport of 5.3 Sv of IcSPMW in the Irminger Sea. These 5.3 Sv combine with 1.1 Sv of Central  
802 Waters and 2.2 Sv of SAIW (crossing over the Reykjanes Ridge) to give 8.8 Sv of IrSPMW through  
803 air–sea interaction.

804 LSW is the main water mass across the sections ( $35.0 \pm 0.6$  % of the section volume). The  
805 inter-annual variability observed in the upper layers of the Irminger Basin reflects the interplay  
806 between LSW and SPMW, the mixing of which emulates the presence of the upper LSW. In the  
807 lower layers at both sides of the Reykjanes Ridge it is possible to notice an interaction between  
808 LSW and ISOW, with an increasing presence of ISOW responding to the progressive dilution of  
809 LSW. The OMP results also reveal that LSW is strongly mixed with the surrounding waters mainly  
810 in two regions: (i) at and upstream of the Reykjanes Ridge, and (ii) in the Deep Western Boundary  
811 Current, where the contribution of LSW is significant ( $\sigma_0 > 27.80$ ). The slightly negative net  
812 transport of LSW across the OVIDE section is in agreement with a moderate formation of LSW in  
813 the Irminger Basin.

814 Waters from the ENA Basin cross over the Reykjanes Ridge and enter the Irminger Basin,  
815 where they are transformed and/or densified, passing from the upper and intermediate water  
816 domains to the deep water domain. The OMP analysis allowed us to decompose the 9.4 Sv of flow  
817 across the Reykjanes Ridge into Central Waters, SAIW, LSW and ISOW; SAIW being the main  
818 contributor.

819 The distributions and transports of ISOW allow us to infer that in the course of the ISOW's  
820 journey from the Iceland–Scotland sills to the CGFZ, part of it upwells and flows through gaps in  
821 the Reykjanes Ridge between the OVIDE and 4x sections. Once ISOW arrives at the CGFZ some  
822 fractions continue to flow into the West European Basin while the main stream crosses the fracture  
823 to the Irminger Basin, flowing northwards and joining the fractions that previously crossed the  
824 ridge.

825 The extension of this methodology to wide areas of the ocean could provide a useful basis  
826 for this kind of study or more ambitious ones dealing with the cycle of biogeochemical components  
827 in the ocean.

828 **Acknowledgements**

829           We are grateful to the captains, staff and researchers who contributed to the acquisition  
830 and data processing. The research leading to these results was supported through the EU FP7  
831 project CARBOCHANGE, which received funding from the European Commission's Seventh  
832 Framework Programme under grant agreement no. 264879. For this work M.I. García-Ibáñez was  
833 supported by the Spanish Ministry of Economy and Competitiveness (BES-2011-045614) through  
834 the CATARINA (CTM2010-17141) and BOCATS projects (CTM2013-41048-P) supported by the  
835 Spanish Government and co-funded by the Fondo Europeo de Desarrollo Regional 2007–2012  
836 (FEDER); and this article is going to be part of her PhD that is attached to the framework of the  
837 doctoral program "Marine Science, Technology and Management" (DO\*MAR) of the University of  
838 Vigo. P.C. Pardo, L.I. Carracedo, A.F. Rios and F.F. Pérez were supported by the Spanish  
839 National Research Council (CSIC); H. Mercier by the French National Centre for Scientific  
840 Research (CNRS); and P. Lherminier by the French Institute for Marine Science (Ifremer).

841 **Appendix**842 **A1. Specifications of the OMP analysis**

843 The Optimum MultiParameter (OMP) analyses consider the properties (physical and/or  
 844 chemical) of a given water sample to be the result of linear combinations of a finite number of  
 845 water masses represented by the so-called Source Water Types (SWT). They compute the  
 846 fractions of each SWT ( $X_i$ ) in each water sample. In the OMP analyses, the SWT properties are  
 847 assumed to be independent and equally affected by mixing. In addition, SWTs are considered to  
 848 be time invariant; hence, changes in the properties of the water masses over time are reflected  
 849 through water mass redistributions.

850 The methodology of the analysis applied in this work consists of two OMP steps. In the first  
 851 step a classical OMP (cOMP) is solved for each water sample. The cOMP analysis is based on  
 852 conservative variables; in particular, in this study we used  $\theta$ , S,  $\text{SiO}_2$ , "NO" and "PO" (where "NO" =  
 853  $10.5 * \text{NO}_3 + \text{O}_2$ , "PO" =  $175 * \text{PO}_4 + \text{O}_2$ ; Broecker, 1974; Takahashi et al., 1985; Anderson and  
 854 Sarmiento, 1994):

$$\begin{aligned}
 \sum_{i=1}^n X_i * \theta_i^{\text{SWT}} &= \theta^{\text{sample}} + R_\theta \\
 \sum_{i=1}^n X_i * S_i^{\text{SWT}} &= S^{\text{sample}} + R_S \\
 \sum_{i=1}^n X_i * \text{SiO}_{2i}^{\text{SWT}} &= \text{SiO}_2^{\text{sample}} + R_{\text{SiO}_2} \\
 \sum_{i=1}^n X_i * \text{NO}_i^{\text{SWT}} &= \text{NO}^{\text{sample}} + R_{\text{NO}} \\
 \sum_{i=1}^n X_i * \text{PO}_i^{\text{SWT}} &= \text{PO}^{\text{sample}} + R_{\text{PO}} \\
 \sum_{i=1}^n X_i &= 1 + R_{\text{mass}}
 \end{aligned} \quad (\text{Eq. A1.1})$$

856 where  $R_p$  is the residual of each property  $p$  ( $\theta$ , S,  $\text{SiO}_2$ , NO and PO) measured ( $p^{\text{sample}}$ )  
 857 that the OMP tries to minimize and  $p_i^{\text{SWT}}$  is the property of each SWT  $i$ . The last equation accounts  
 858 for the mass conservation. Before solving the system (minimization through a non-negative least  
 859 square method), the equations are normalized (Tomczak and Large, 1989) and weighted (Pardo et  
 860 al., 2012) (Table 2). The assignment of weights was, as a first step, directly related to the accuracy  
 861 of the property and/or to the variability in the region of study. Weights were also adjusted so that  
 862 the ratios between the Standard Deviations of the Residuals and the analytical error ( $\epsilon$ , accuracy of  
 863 the measured properties) were almost the same for all the SWT properties (Table 2). The weights  
 864 of  $\theta$  and S are higher than those of the other properties because both have the lowest  $\epsilon$ . The mass  
 865 equation has the highest weight to ensure its conservation.

866 The cOMP analysis is solved for each mixing *figure*. The mixing *figures* are groups of SWTs  
 867 that are susceptible to mix together, and are set considering the vertical characteristics and/or  
 868 dynamics of the SWTs in the region of study. Each mixing *figure* is constituted by a maximum of  
 869 four SWTs in order to solve the system of 6 equations with at least two degrees of freedom (Eq.  
 870 A1.1). The mixing *figures* are vertically and horizontally sequenced, sharing at least one SWT with  
 871 the adjacent mixing *figures*. The cOMP analysis is applied to assign the mixing *figure* where the  
 872 water sample is best included (lowest residuals).

873 In the second step an extended OMP (eOMP) analysis is solved with the same set-up as  
 874 the cOMP except that the eOMP considers conservative and non-conservative variables. We used  
 875  $\theta$  and S as conservative variables and  $\text{SiO}_2$ ,  $\text{NO}_3$ ,  $\text{PO}_4$  and  $\text{O}_2$  as non-conservative variables. A  
 876 new unknown has to be considered,  $\Delta\text{O}$ , in order to account for the biogeochemical process of  
 877 remineralisation of the organic matter. The system of equations remains as follows:

$$\begin{aligned}
 \sum_{i=1}^n X_i * \theta_i^{\text{SWT}} &= \theta^{\text{sample}} + R_{\theta} \\
 \sum_{i=1}^n X_i * S_i^{\text{SWT}} &= S^{\text{sample}} + R_S \\
 \sum_{i=1}^n X_i * \text{SiO}_{2i}^{\text{SWT}} + \Delta\text{O}/r_{\text{Si}} &= \text{SiO}_2^{\text{sample}} + R_{\text{SiO}_2} \\
 \sum_{i=1}^n X_i * \text{O}_{2i}^{\text{SWT}} - \Delta\text{O} &= \text{O}_2^{\text{sample}} + R_{\text{O}_2} \quad (\text{Eq. A1.2}) \\
 \sum_{i=1}^n X_i * \text{NO}_{3i}^{\text{SWT}} + \Delta\text{O}/r_{\text{N}} &= \text{NO}_3^{\text{sample}} + R_{\text{NO}_3} \\
 \sum_{i=1}^n X_i * \text{PO}_{4i}^{\text{SWT}} + \Delta\text{O}/r_{\text{P}} &= \text{PO}_4^{\text{sample}} + R_{\text{PO}_4} \\
 \sum_{i=1}^n X_i &= 1 + R_{\text{mass}}
 \end{aligned}$$

879 where  $r_{\text{Si}}$  is 12,  $r_{\text{N}}$  is 10.5 and  $r_{\text{P}}$  is 175 (Takahashi et al., 1985; Anderson and Sarmiento,  
 880 1994).

881 The final result from the eOMP analysis is the  $X_i$ s in each water sample in the  
 882 corresponding mixing *figure* selected through the cOMP analysis.

883 The cOMP analysis selects the mixing *figure* based on conservative water mass tracers,  
 884 avoiding the complexity added by the non-conservative variables. Even though this analysis does  
 885 not consider the variability associated with biological processes, it is accurate enough to select the  
 886 appropriate mixing *figure*. Once the mixing *figures* are selected, the estimates of the  $X_i$ s are given  
 887 by the eOMP analysis, which does take into account the effect of the biology in the measured  
 888 variables.

889 **A2. Testing the robustness: perturbation analysis of uncertainties**

890 The robustness of the OMP analysis was tested through a perturbation analysis of  
891 uncertainties (Lawson and Hanson, 1974). In this work, the properties of both each SWT and each  
892 water sample were perturbed. This allowed us to check the sensitivity of the model to variations in  
893 the SWTs, due to environmental variability, and in the water samples, due to measurement errors  
894 (Leffanue and Tomczak, 2004).

895 To apply this procedure, it is assumed that the property distributions follow a normal  
896 distribution constructed with the mean equal to the property value at each point and a standard  
897 deviation (STD) (Álvarez et al., 2004; Pardo et al., 2012). The perturbation process lies in varying  
898 the property values within the normal distribution. All the STDs used in perturbing the SWTs are  
899 shown in Table 2.

900 The STDs of the water sample properties ( $\varepsilon$  in Table 2) were obtained by considering  $\varepsilon$   
901 almost equal to the accuracy of each water sample property ( $\varepsilon_{\theta}$  0.01,  $\varepsilon_S$  0.01,  $\varepsilon_{SiO_2}$  0.3,  $\varepsilon_{NO_3}$  0.2,  
902  $\varepsilon_{PO_4}$  0.02 and  $\varepsilon_{O_2}$  1). The STDs of the properties of the SWTs were obtained within the realm of the  
903 SWT ( $X_i > 75\text{-}95\%$ ) by one of the following methods:

904 a) Following Karstensen and Tomczak (1998), the water samples with more than 95 % of  
905 contribution of a certain SWT ( $X_i$ ) were selected and the STD calculated for each property.  
906 This method was only used when the number of water samples that could be selected for a  
907 certain SWT was more than 50. This procedure was applied to LSW, ISOW and NEADW<sub>L</sub>.

908 b) For the water masses that were modelled by various SWTs (multi-SWTs), as the Central  
909 Waters, DSOW and SPMW, the multi-SWT contributions were obtained by adding the  
910 contributions of their respective components. Then the water samples with  $X_i$  of the multi-  
911 SWT greater than 95 % were selected. The property values of each component of the multi-  
912 SWT were then subtracted from the values of the water samples and linear regressions  
913 between  $\theta$  and the rest of the resulting properties were performed. The STDs of the multi-  
914 SWT properties were assumed to be equal to the error of the intercept. The properties of  
915 each component of the multi-SWT had the same STDs as the corresponding ones in the  
916 multi-SWT. With this methodology the variability due to the  $\theta$  variability was removed.

917 c) A modification of the methodology in (b) was applied to MW, where samples with  $X_i > 75\%$   
918 were selected and used for the linear regressions.

919 The STDs of the properties of SAIW were assigned equal to those of the Central Waters,  
920 because not enough water samples presented  $X_i > 95\%$  of this water mass. The STD of NEADW<sub>U</sub>  
921 was computed using the errors of the SWTs in which it is assumed to decompose (section 3).

922 We set the STDs for the O<sub>2</sub> as a value equal to 3 % of the saturation value, since when a  
923 water mass is formed the content of O<sub>2</sub> is not exactly the saturation value (Najjar and Keeling,  
924 2000; Ito et al., 2004).

925 100 perturbations were performed and the OMP analysis was solved for each perturbed  
926 system. Uncertainties in the  $X_i$ s are computed from the results of the perturbations. We calculated  
927 the STD of the 100 SWT distribution matrixes. The mean of the STD matrix is shown in Table 2.  
928 The SWTs with higher mean STD values are those that belong to a mixing *figure* that covers a  
929 small property range, where the variability of the SWTs has a greater effect.

### 930 **A3. Testing the accuracy: residuals**

931 The least square method constrained to non-negative solutions returns the total residual,  
932 i.e., the squared largest singular value for the set of residuals resulting from the eOMP equation  
933 system (section A1). These residuals give insights about the reliability of the proposed mixing  
934 model, and indicate the quality of the solution for each depth range. The total and individual  
935 residuals for the water samples are shown in Fig. A3.1.

936 The total residual of the eOMP analysis is almost zero from 500 m depth to the bottom (Fig.  
937 A3.1a). The individual residuals present the same pattern (Fig. A3.1b, c, d). In the surface layer,  
938 the assumption of conservativeness is not justified because this layer is subject to seasonal  
939 variability. Nevertheless, as  $\theta$  and S have the highest weights in the analysis (Table 2), the  
940 majority of the positive residuals of  $\theta$  in the surface–subsurface layer are compensated by the  
941 corresponding negative residuals of S.

942 The model is proved to be reliable since it explains almost 99 % of the variability of the  
943 conservative tracers, and more than 97 % of all the non-conservative tracers except PO<sub>4</sub> (94 %)

944 (Table 2). The Standard Deviations of the Residuals provide an estimation of the goodness of our  
945 proposed mixing model.

946 **References**

- 947 Álvarez, M., Bryden, H.L., Pérez, F.F., Ríos, A.F., Rosón, G., 2002. Physical and biogeochemical  
948 fluxes and net budgets in the subpolar and temperate North Atlantic. *Journal of Marine*  
949 *Research* 60, 191-226. doi: 10.1357/00222400260497462.
- 950 Álvarez, M., Brea, S., Mercier, H., Álvarez-Salgado, X.A., 2014. Mineralization of biogenic  
951 materials in the water masses of the South Atlantic Ocean. I: Assessment and results of an  
952 optimum multiparameter analysis. *Progress in Oceanography* 123, 1-23. doi:  
953 10.1016/j.pocean.2013.12.007.
- 954 Álvarez, M., Pérez, F.F., Bryden, H., Ríos, A.F., 2004. Physical and biogeochemical transports  
955 structure in the North Atlantic subpolar gyre. *Journal of Geophysical Research* 109,  
956 C03027. doi: 10.1029/2003JC002015.
- 957 Ambar, I., Howe, M.R., 1979. Observations of the Mediterranean outflow-I: Mixing in the  
958 Mediterranean outflow. *Deep Sea Research Part A. Oceanographic Research Papers* 26,  
959 5, 535-554. doi: 10.1016/0198-0149(79)90095-5.
- 960 Aminot, A., Chaussepied, M., 1983. Manuel des analyses chimiques en Milieu Marin. Publications  
961 du CNEXO, 395p.
- 962 Anderson, L.A., Sarmiento, J.L., 1994. Redfield ratios of remineralization determined by nutrient  
963 data analysis. *Global Biogeochemical Cycles* 8, 1, 65-80. doi: 10.1029/93GB03318.
- 964 Arhan, M., 1990. The North Atlantic Current and subarctic intermediate water. *Journal of Marine*  
965 *Research* 48, 1, 109-144. doi: 10.1357/002224090784984605.
- 966 Arhan, M., Colin de Verdière, A., Mémery, L., 1994. The eastern boundary of the subtropical North  
967 Atlantic. *Journal of Physical Oceanography* 24, 6, 1295-1316. doi: 10.1175/1520-  
968 0485(1994)024<1295:TEBOTS>2.0.CO;2.
- 969 Arhan, M., King, B., 1995. Lateral mixing of the Mediterranean Water in the eastern North Atlantic.  
970 *Journal of Marine Research* 53, 6, 865-895. doi: 10.1357/0022240953212990.
- 971 Bacon, S., 1997. Circulation and Fluxes in the North Atlantic between Greenland and Ireland.  
972 *Journal of Physical Oceanography* 27, 1420-1435. doi: 10.1175/1520-  
973 0485(1997)027<1420:CAFITN>2.0.CO;2.

- 974 Balmeda, M.A., Smith, G.C., Haines, K., Anderson, D., Palmer, T.N., Vidard, A., 2007. Historical  
975 reconstruction of the Atlantic Meridional Overturning Circulation from the ECMWF  
976 operational ocean reanalysis. *Geophysical Research Letters* 34, L23615. doi:  
977 10.1029/2007GL031645.
- 978 Baringer, M.O., Price, J.F., 1997. Mixing and Spreading of the Mediterranean Outflow. *Journal of*  
979 *Physical Oceanography* 27, 8, 1654-1677. doi: 10.1175/1520-  
980 0485(1997)027<1654:MASOTM>2.0.CO;2.
- 981 Bersch, M., 2002. North Atlantic Oscillation-induced changes of the upper layer circulation in the  
982 northern North Atlantic Ocean. *Journal of Geophysical Research* 107, C10, 3156. doi:  
983 10.1029/2001JC000901.
- 984 Bersch, M., Meincke, J., Sy, A., 1999. Interannual thermohaline changes in the northern North  
985 Atlantic 1991-1996. *Deep Sea Research Part II: Topical Studies in Oceanography* 46, (1-2),  
986 55-75. doi: 10.1016/S0967-0645(98)00114-3.
- 987 Bersch, M., Yashayaev, I., Koltermann, K.P., 2007. Recent changes of the thermohaline circulation  
988 in the subpolar North Atlantic. *Ocean Dynamics* 57, 3, 223-235. doi: 10.1007/s10236-007-  
989 0104-7.
- 990 Böning, C.W., Bryan, F.O., Holland, W.R., Döscher, R., 1996. Deep-Water Formation and  
991 Meridional Overturning in a High-Resolution Model of the North Atlantic. *Journal of Physical*  
992 *Oceanography* 26, 1142-1164. doi: 10.1175/1520-  
993 0485(1996)026<1142:DWFAMO>2.0.CO;2.
- 994 Böning, C.W., Scheinert, M., Dengg, J., Biastoch, A., Funk, A., 2006. Decadal variability of  
995 subpolar gyre transport and its reverberation in the North Atlantic overturning. *Geophysical*  
996 *Research Letters* 33, L21S01. doi: 10.1029/2006GL026906.
- 997 Branellec, P., Thierry V., 2013. OVIDE 2010 CTD-O<sub>2</sub> cruise report.  
998 <http://archimer.ifremer.fr/doc/00210/32134>.
- 999 Brambilla, E., Talley, L.D., 2008. Subpolar Mode Water in the northeastern Atlantic: 1. Averaged  
1000 properties and mean circulation. *Journal of Geophysical Research* 113, C04025. doi:  
1001 10.1029/2006JC004062.

- 1002 Brambilla, E., Talley, L.D., Robbins, P.E., 2008. Subpolar Mode Water in the northeastern Atlantic:  
1003 2. Origin and transformation. *Journal of Geophysical Research* 113, C4, C04026. doi:  
1004 10.1029/2006JC004063.
- 1005 Broecker, W.S., 1974. "NO", a conservative water-mass tracer. *Earth and Planetary Science*  
1006 *Letters* 23, 1, 100-107. doi: 10.1016/0012-821X(74)90036-3.
- 1007 Bryden, H.L., King, B.A., McCarthy, G.D., McDonagh, E.L., 2014. Impact of a 30% reduction in  
1008 Atlantic meridional overturning during 2009-2010. *Ocean Science* 10, 683-691. doi:  
1009 10.5194/os-10-683-2014.
- 1010 Bubnov, V.A., 1968. Intermediate subarctic waters in the northern part of the Atlantic Ocean.  
1011 *Okeanologia* 19, 136-153 (English translation, N00 Trnas 545, U.S. Nav. Oceanogr. Off.,  
1012 Washington, D. C., 1973).
- 1013 Carracedo, L.I., Gilcoto, M., Mercier, H., Pérez, F.F., 2014. Seasonal dynamics in the Azores-  
1014 Gibraltar Strait region: A climatologically-based study. *Progress in Oceanography* 122, 116-  
1015 130. doi: 10.1016/j.pocean.2013.12.005.
- 1016 Carracedo, L.I., Pardo, P.C., Villacieros-Robineau, N., De la Granda, F., Gilcoto, M., Pérez, F.F.,  
1017 2012. Temporal changes in the water mass distribution and transports along the 20°W  
1018 CAIBOX section (NE Atlantic). *Ciencias Marinas* 38, 1B, 263-286. doi:  
1019 10.7773/cm.v38i1B.1793.
- 1020 Castro, C.G., Pérez, F.F., Holley, S.E., Ríos, A.F., 1998. Chemical characterisation and modelling  
1021 of water masses in the Northeast Atlantic. *Progress in Oceanography* 41, 249-279. doi:  
1022 10.1016/S0079-6611(98)00021-4.
- 1023 Clarke, R.A., 1984. Transport through the Cape Farewell-Flemish Cap section. *Rapp. PV Reun.*  
1024 *Cons. Int. Explor. Mer*, 185, 120-130.
- 1025 Culberson, C.H., 1991. WOCE operations manual (WHP operations and methods), WHPO 91/1.  
1026 Woods Hole Oceanogr. Inst., Woods Hole, Mass.
- 1027 Cunningham, S.A., Haine, T.W.N., 1995. Labrador Sea Water in the eastern North Atlantic. Part II:  
1028 Mixing dynamics and the advective-diffusive balance. *Journal of Physical Oceanography*  
1029 14, 103-127. doi: 10.1175/1520-0485(1995)025<0666:LSWITE>2.0.CO;2.

- 1030 Curry, R.G., McCartney, M.S., 2001. Ocean Gyre Circulation Changes Associated with the North  
1031 Atlantic Oscillation\*. *Journal of Physical Oceanography* 31, 3374-3400. doi: 10.1175/1520-  
1032 0485(2001)031<3374:OGCCAW>2.0.CO;2.
- 1033 Daniault, N., Lherminier, P., Mercier, H., 2011. Circulation and transport at the southeast tip of  
1034 Greenland. *Journal of Physical Oceanography* 41, 3, 437-457. doi:  
1035 10.1175/2010JPO4428.1.
- 1036 de Boissésou, E., Thierry, V., Mercier, H., Caniaux, G., Desbruyères, D., 2012. Origin, formation  
1037 and variability of the Subpolar Mode Water located over the Reykjanes Ridge. *Journal of*  
1038 *Geophysical Research* 117, C12005. doi: 10.1029/2011JC007519.
- 1039 de Jong, M.F., van Aken, H.M., Våge, K., Pickart, R.S., 2012. Convective mixing in the central  
1040 Irminger Sea: 2002-2010. *Deep Sea Research Part I: Oceanographic Research Papers* 63,  
1041 36-51. doi: 10.1016/j.dsr.2012.01.003.
- 1042 Dengler, M., Fischer, J., Schott, F.A., Zantopp R., 2006. Deep Labrador Current and its variability  
1043 in 1996-2005. *Geophys. Research Letters* 33, L21S06. doi: 10.1029/2006GL026702.
- 1044 Desbruyères, D., Thierry, V., Mercier, H., 2013. Simulated decadal variability of the meridional  
1045 overturning circulation across the A25-Ovide section. *Journal of Geophysical Research*  
1046 *Oceans* 118, 462-475. doi: 10.1029/2012JC008342.
- 1047 Dickson, B., Yashayaev, I., Meincke, J., Turrell, B., Dye, S., Holfort, J., 2002. Rapid freshening of  
1048 the deep North Atlantic Ocean over the past four decades. *Nature* 416, 6883, 832-837. doi:  
1049 10.1038/416832a.
- 1050 Dickson, R., Lazier, J., Meincke, J., Rhines, P., Swift, J., 1996. Long-term coordinated changes in  
1051 the convective activity of the North Atlantic. *Progress in Oceanography* 38, 3, 241-295. doi:  
1052 10.1016/S0079-6611(97)00002-5.
- 1053 Dickson, R.R., Brown, J., 1994. The production of North Atlantic Deep Water: sources, rates, and  
1054 pathways. *Journal of Geophysical Research* 99, C6, 12319-12. doi: 10.1029/94JC00530.
- 1055 Eden, C., Willebrand, J., 2001. Mechanism of Interannual to Decadal Variability of the North  
1056 Atlantic Circulation. *Journal of Climate* 14, 2266-2280. doi: 10.1175/1520-  
1057 0442(2001)014<2266:MOITDV>2.0.CO;2.

- 1058 Falina, A., Sarafanov, A., Mercier, H., Lherminier, P., Sokov, A., Daniault, N., 2012. On the  
1059 Cascading of Dense Shelf Waters in the Irminger Sea. *Journal of Physical Oceanography*  
1060 42, 2254-2267. doi: 10.1175/JPO-D-12-012.1.
- 1061 Ferron, B., Kokoszka, F., Mercier, H., Lherminier, P., 2014. Dissipation rate estimates from  
1062 microstructure and finescale internal wave observations along the A25 Greenland-Portugal  
1063 OVIDE line. *Journal of Atmospheric and Oceanic Technology* 31, 2530-2543. doi:  
1064 10.1175/JTECH-D-14-00036.1.
- 1065 Flatau, M.K., Talley, L., Niiler, P.P., 2003. The North Atlantic Oscillation, Surface Current  
1066 Velocities, and SST Changes in the Subpolar North Atlantic. *Journal of Climate* 16, 2355-  
1067 2369. doi: 10.1175/2787.1.
- 1068 Fogelqvist, E., Blindheim, J., Tanhua, T., Østerhus, S., Buch, E., Rey, F., 2003. Greenland-  
1069 Scotland overflow studied by hydro-chemical multivariate analysis. *Deep Sea Research*  
1070 Part I: Oceanographic Research Papers 50, 1, 73-102. doi: 10.1016/S0967-  
1071 0637(02)00131-0.
- 1072 Gourcuff, C., Lherminier, P., Mercier, H., Le Traon, P.Y., 2011. Altimetry Combined with  
1073 Hydrography for Ocean Transport Estimation. *Journal of Atmospheric and Oceanic*  
1074 *Technology* 28, 10, 1324-1337. doi: 10.1175/2011JTECHO818.1.
- 1075 Häkkinen, S., Rhines, P.B., 2004. Decline of subpolar North Atlantic circulation during the 1990s.  
1076 *Science* 304, 5670, 555-559. doi: 10.1126/science.1094917.
- 1077 Hansen, B., Østerhus, S., 2000. North Atlantic-nordic seas exchanges. *Progress in Oceanography*  
1078 45, 2, 109-208. doi: 10.1016/S0079-6611(99)00052-X.
- 1079 Harvey, J., 1982. Theta-S relationships and water masses in the eastern North Atlantic. *Deep Sea*  
1080 *Research Part A. Oceanographic Research Papers* 29, 8, 1021-1033. doi: 10.1016/0198-  
1081 0149(82)90025-5.
- 1082 Harvey, J., Arhan, M., 1988. The water masses of the central North Atlantic in 1983-84. *Journal of*  
1083 *Physical Oceanography* 18, 12, 1855-1875. doi: 10.1175/1520-  
1084 0485(1988)018<1855:TWMOTC>2.0.CO;2.

- 1085 Hátún, H., Sandø, A.B., Drange, H., Hansen, B., Valdimarsson, H., 2005. Influence of the Atlantic  
1086 subpolar gyre on the thermohaline circulation. *Science* 309, 5742, 1841-1844. doi:  
1087 10.1126/science.1114777.
- 1088 Hurrell, J.W., 1995. Decadal Trends in the North Atlantic Oscillation: Regional Temperatures and  
1089 Precipitation. *Science* 269, 676-679. doi: 10.1126/science.269.5224.676.
- 1090 Iselin, C.O., 1936. A study of the circulation of the western North Atlantic. *Pap. Phys. Oceanogr.*  
1091 *Meteorol. Massachusetts Inst. Tech. and Woods Hole Oceanographic Inst.* 101p.
- 1092 Ito, T., Follows, M.J., Boyle, E.A., 2004. Is AOU a good measure of respiration in the oceans?  
1093 *Geophysical research letters* 31, L17305. doi: 10.1029/2004GL020900.
- 1094 Jochumsen, K., Quadfasel, D., Valdimarsson, H., Jónsson S., 2012. Variability of the Denmark  
1095 Strait overflow: Moored time series from 1996-2011. *Journal of Geophysical Research* 117,  
1096 C12003, doi: 10.1029/2012JC008244.
- 1097 Josey, S.A., Grist, J.P., Marsh, R., 2009. Estimates of meridional overturning circulation variability  
1098 in the North Atlantic from surface density flux fields. *Journal of Geophysical Research* 114,  
1099 C09022. doi: 10.1029/2008JC005230.
- 1100 Karstensen, J., Tomczak, M., 1998. Age determination of mixed water masses using CFC and  
1101 oxygen data. *Journal of Geophysical Research* 103, C9, 18599-18609. doi:  
1102 10.1029/98JC00889.
- 1103 Kieke, D., Rhein, M., Stramma, L., Smethie, W.M., Bullister, J.L., LeBel, D.A., 2007. Changes in  
1104 the pool of Labrador Sea Water in the subpolar North Atlantic. *Geophysical Research*  
1105 *Letters* 34, 6, L06605. doi: 10.1029/2006GL028959.
- 1106 Krauss, W., 1995. Currents and mixing in the Irminger Sea and in the Iceland Basin. *Journal of*  
1107 *Geophysical Research* 100, C6, 10851-10871. doi: 10.1029/95JC00423.
- 1108 Lawson, C.L., Hanson, R.J., 1974. Solving least squares problems. *Society for Industrial and*  
1109 *Applied Mathematics (SIAM)*. 351p.
- 1110 Lazier, J., Hendry, R., Clarke, A., Yashayaev, I., Rhines, P., 2002. Convection and restratification  
1111 in the Labrador Sea, 1990-2000. *Deep Sea Research Part I: Oceanographic Research*  
1112 *Papers* 49, 10, 1819-1835. doi: 10.1016/S0967-0637(02)00064-X.

- 1113 Lazier, J.R.N., 1973. The renewal of Labrador Sea Water. Deep Sea Research and  
1114 Oceanographic Abstracts 20, 4, 341-353. doi: 10.1016/0011-7471(73)90058-2.
- 1115 Leffanue, H., Tomczak, M., 2004. Using OMP analysis to observe temporal variability in water  
1116 mass distribution. Journal of marine systems 48, 1, 3-14. doi:  
1117 10.1016/j.jmarsys.2003.07.004.
- 1118 Lherminier, P., Mercier, H., Gourcuff, C., Alvarez, M., Bacon, S., Kermabon, C., 2007. Transports  
1119 across the 2002 Greenland-Portugal Ovide section and comparison with 1997. Journal of  
1120 Geophysical Research 112, C7, C07003. doi: 10.1029/2006JC003716.
- 1121 Lherminier, P., Mercier, H., Huck, T., Gourcuff, C., Perez, F.F., Morin, P., Sarafanov, A., Falina, A.,  
1122 2010. The Atlantic Meridional Overturning Circulation and the subpolar gyre observed at  
1123 the A25-OVIDE section in June 2002 and 2004. Deep Sea Research Part I: Oceanographic  
1124 Research Papers 57, 11, 1374-1391. doi: 10.1016/j.dsr.2010.07.009.
- 1125 Mackas, D.L., Denman, K.L., Bennett, A.F., 1987. Least squares multiple tracer analysis of water  
1126 mass composition. Journal of Geophysical Research 92, C3, 2907-2918. doi:  
1127 10.1029/JC092iC03p02907.
- 1128 Macrander, A., Send, U., Valdimarsson, H., Jónsson, S., Käse, R.H., 2005. Interannual changes in  
1129 the overflow from the Nordic Seas into the Atlantic Ocean through Denmark Strait.  
1130 Geophysical Research Letters 32, 6, L06606. doi: 10.1029/2004GL021463.
- 1131 Malmberg, S.A., 1972. Intermediate Polar Water in the Denmark Strait Overflow August 1971.  
1132 ICES Conf. Meet. 6, 44-60.
- 1133 Mantyla, A.W., 1994. The treatment of inconsistencies in Atlantic deep water salinity data. Deep  
1134 Sea Research Part I: Oceanographic Research Papers 41, 9, 1387-1405. doi:  
1135 10.1016/0967-0637(94)90104-X.
- 1136 Marsh, R., de Cuevas, B.A., Coward, A.C., Bryden, H.L., Álvarez, M., 2005. Thermohaline  
1137 circulation at three key sections in the North Atlantic over 1985-2002. Geophysical  
1138 Research Letters 32, L10604. doi: 10.1029/2004GL022281.
- 1139 Mazé, J.P., Arhan, M., Mercier, H., 1997. Volume budget of the eastern boundary layer off the  
1140 Iberian Peninsula. Deep Sea Research Part I: Oceanographic Research Papers 44, 9-10,  
1141 1543-1574. doi: 10.1016/S0967-0637(97)00038-1.

- 1142 McCartney, M.S., Mauritzen, C., 2001. On the origin of the warm inflow to the Nordic Seas.  
1143 Progress in Oceanography 51, 1, 125-214. doi: 10.1016/S0079-6611(01)00084-2.
- 1144 McCartney, M.S., Talley, L.D., 1982. The subpolar mode water of the North Atlantic Ocean.  
1145 Journal of Physical Oceanography 12, 11, 1169-1188. doi: 10.1175/1520-  
1146 0485(1982)012<1169:TSMWOT>2.0.CO;2.
- 1147 Mercier, H., 1986. Determining the general circulation of the ocean: A nonlinear inverse problem.  
1148 Journal of Geophysical Research 91, C4, 5103-5109. doi: 10.1029/JC091iC04p05103.
- 1149 Mercier, H., Lherminier, P., Sarafanov, A., Gaillard, F., Danialt, N., Desbruyères, D., Falina, A.,  
1150 Ferron, B., Gourcuff, C., Huck, T., 2015. Variability of the meridional overturning circulation  
1151 at the Greenland-Portugal OVIDE section from 1993 to 2010. Progress in Oceanography  
1152 91, C4, 5103-5109. doi: 10.1016/j.pocean.2013.11.001.
- 1153 Najjar, R.G., Keeling, R.F., 2000. Mean annual cycle of the air-sea oxygen flux: A global view.  
1154 Global Biogeochemical Cycles 14, 2, 573-584. doi: 10.1029/1999GB900086.
- 1155 New, A.L., Barnard, S., Herrmann, P., Molines, J.-M., 2001. On the origin and pathway of the  
1156 saline inflow to the Nordic Seas: insights from models. Progress in Oceanography 48, 2-3,  
1157 255-287. doi: 10.1016/S0079-6611(01)00007-6.
- 1158 Olsen, S.M., Hansen, B., Quadfasel, D., Østerhus, S., 2008. Observed and modelled stability of  
1159 overflow across the Greenland-Scotland ridge. Nature 455, 519-522. doi:  
1160 10.1038/nature07302.
- 1161 Olsson, K.A., Jeansson, E., Tanhua, T., Gascard, J.-C., 2005. The East Greenland Current studied  
1162 with CFCs and released sulphur hexafluoride. Journal of Marine Systems 55, 1, 77-95. doi:  
1163 10.1016/j.jmarsys.2004.07.019.
- 1164 Paillet, J., Arhan, M., McCartney, M.S., 1998. Spreading of Labrador Sea Water in the eastern  
1165 North Atlantic. Journal of Geophysical Research 103, C5, 10223-10239. doi:  
1166 10.1029/98JC00262.
- 1167 Pardo, P.C., Pérez, F.F., Velo, A., Gilcoto, M., 2012. Water masses distribution in the Southern  
1168 Ocean: Improvement of an extended OMP (eOMP) analysis. Progress in Oceanography  
1169 103, 92-105. doi: 10.1016/j.pocean.2012.06.002.

- 1170 Pérez, F.F., Mercier, H., Vázquez-Rodríguez, M., Lherminier, P., Velo, A., Pardo, P.C., Rosón, G.,  
1171 Ríos, A.F., 2013. Atlantic Ocean CO<sub>2</sub> uptake reduced by weakening of the meridional  
1172 overturning circulation. *Nature Geoscience* 6, 2, 146-152. doi: 10.1038/ngeo1680.
- 1173 Pickart, R.S., 1992. Water mass components of the North Atlantic deep western boundary current.  
1174 *Deep Sea Research Part A. Oceanographic Research Papers* 39, 9, 1553-1572. doi:  
1175 10.1016/0198-0149(92)90047-W.
- 1176 Pickart, R.S., Smethie Jr., W.M., Lazier, J.R.N., Jones, E.P., Jenkins, W.J., 1996. Eddies of newly  
1177 formed upper Labrador Sea water. *Journal of Geophysical Research* 101, C9, 20711-  
1178 20726. doi: 10.1029/96JC01453.
- 1179 Pickart, R.S., Straneo, F., Moore, G.K., 2003. Is Labrador Sea Water formed in the Irminger basin?  
1180 *Deep Sea Research Part I: Oceanographic Research Papers* 50, 1, 23-52. doi:  
1181 10.1016/S0967-0637(02)00134-6.
- 1182 Pickart, R.S., Torres, D.J., Fratantoni, P.S., 2005. The East Greenland Spill Jet. *Journal of*  
1183 *Physical Oceanography* 35, 1037-1053. doi: 10.1175/JPO2734.1.
- 1184 Pollard, R.T., Griffthts, M.J., Cunningham, S.A., Read, J.F., Pérez, F.F., Ríos, A.F., 1996. Vivaldi  
1185 1991 - A study of the formation, circulation and ventilation of Eastern North Atlantic Central  
1186 Water. *Progress in Oceanography* 37, 167-192. doi: 10.1016/S0079-6611(96)00008-0.
- 1187 Pollard, R.T., Read, J.F., Holliday, N.P., Leach, H., 2004. Water masses and circulation pathways  
1188 through the Iceland Basin during Vivaldi 1996. *Journal of Geophysical Research* 109,  
1189 C04004. doi: 10.1029/2003JC002067.
- 1190 Read, J.F., 2000. CONVEX-91: water masses and circulation of the Northeast Atlantic subpolar  
1191 gyre. *Progress in Oceanography* 48, 4, 461-510. doi: 10.1016/S0079-6611(01)00011-8.
- 1192 Reid, J.L., 1979. On the contribution of the Mediterranean Sea outflow to the Norwegian-  
1193 Greenland Sea. *Deep Sea Research Part A. Oceanographic Research Papers* 26, 11,  
1194 1199-1223. doi: 10.1016/0198-0149(79)90064-5.
- 1195 Rhein, M., Fischer, J., Smethie, W.M., Smythe-Wright, D., Weiss, R.F., Mertens, C., Min, D.-H.,  
1196 Fleischmann, U., Putzka, A., 2002. Labrador Sea Water: Pathways, and formation rates.  
1197 *Journal of Physical Oceanography* 32, 648-665. doi: 10.1175/1520-  
1198 0485(2002)0322.0.CO;2.

- 1199 Ross, C.K., 1984. Temperature-salinity characteristics of the “overflow” water in Denmark Strait  
1200 during “OVERFLOW’73.” *Rapp. PV Reun. Cons. Int. Explor. Mer* 185, 111-119.
- 1201 Rudels, B., Fahrbach, E., Meincke, J., Budéus, G., Eriksson, P., 2002. The East Greenland  
1202 Current and its contribution to the Denmark Strait overflow. *ICES Journal of Marine*  
1203 *Science: Journal du Conseil* 59, 6, 1133-1154. doi: 10.1006/jmsc.2002.1284.
- 1204 Sarafanov, A., 2009. On the effect of the North Atlantic Oscillation on temperature and salinity of  
1205 the subpolar North Atlantic intermediate and deep waters. *ICES Journal of Marine Science*  
1206 66, 7, 1448-1454. doi: 10.1093/icesjms/fsp094.
- 1207 Sarafanov, A., Falina, A., Mercier, H., Sokov, A., Lherminier, P., Gourcuff, C., Gladyshev, S.,  
1208 Gaillard, F., Daniault, N., 2012. Mean full-depth summer circulation and transports at the  
1209 northern periphery of the Atlantic Ocean in the 2000s. *Journal of Geophysical Research*  
1210 117, C1, C01014. doi: 10.1029/2011JC007572.
- 1211 Sarafanov, A., Mercier, H., Falina, A., Sokov, A., Lherminier, P., 2010. Cessation and partial  
1212 reversal of deep water freshening in the northern North Atlantic: observation-based  
1213 estimates and attribution. *Tellus A* 62, 1, 80-90. doi: 10.1111/j.1600-0870.2009.00418.x.
- 1214 Saunders, P.M., 1986. The accuracy of measurements of salinity, oxygen and temperature in the  
1215 deep ocean. *Journal of Physical Oceanography* 16, 189-195. doi: 10.1175/1520-  
1216 0485(1986)016<0189:TAOMOS>2.0.CO;2.
- 1217 Saunders, P.M., 1996. The Flux of Dense Cold Overflow Water Southeast of Iceland. *Journal of*  
1218 *Physical Oceanography* 26, 1, 85-95. doi: 10.1175/1520-  
1219 0485(1996)026<0085:TFODCO>2.0.CO;2.
- 1220 Saunders, P.M., 2001. The dense northern overflows, in: *Ocean Circulation and Climate*, Edited by  
1221 G. Siedler, J. Church, and J. Gould. Academic, New York, pp. 401-417.
- 1222 Schmitz Jr, W., 1996. On the World Ocean Circulation: Volume I: some global features/North  
1223 Atlantic Circulation. Woods Hole Oceanogr. Inst. Tech. Rep. WHOI-96-03, 150 p. [Available  
1224 from Woods Hole Oceanographic Institution, Woods Hole, MA 02543].
- 1225 Schmitz, J.W.J., McCartney, M.S., 1993. On the North Atlantic Circulation. *Reviews of Geophysics*  
1226 31, 1, 29-49. doi: 10.1029/92RG02583.

- 1227 Schott, F.A., Brandt, P., 2007. Circulation and deep water export of the subpolar North Atlantic  
1228 during the 1990s, in *Ocean Circulation: Mechanisms and Impacts*. Geophys. Monogr. Ser.,  
1229 vol. 173, edited by A. Schmittner, J. Chiang, and S. Hemmings, pp. 91-118, AGU,  
1230 Washington, D.C., doi: 10.1029/173GM08.
- 1231 Stoll, M.H.C., van Aken, H.M., de Baar, H.J.W., Kraak, M., 1996. Carbon dioxide characteristics of  
1232 water masses in the northern North Atlantic Ocean. *Marine Chemistry* 55, 3-4, 217-232.  
1233 doi: 10.1016/S0304-4203(96)00058-8.
- 1234 Stramma, L., Kieke, D., Rhein, M., Schott, F., Yashayaev, I., Koltermann, K.P., 2004. Deep water  
1235 changes at the western boundary of the subpolar North Atlantic during 1996 to 2001. *Deep*  
1236 *Sea Research Part I: Oceanographic Research Papers* 51, 8, 1033-1056. doi:  
1237 10.1016/j.dsr.2004.04.001.
- 1238 Sutherland, D.A., Pickart, R.S., 2008. The East Greenland Coastal Current: Structure, variability,  
1239 and forcing. *Progress in Oceanography* 78, 58-77. doi:10.1016/j.pocean.2007.09.006.
- 1240 Takahashi, T., Broecker, W.S., Langer, S., 1985. Redfield ratio based on chemical data from  
1241 isopycnal surfaces. *Journal of Geophysical Research* 90, C4, 6907-6924. doi:  
1242 10.1029/JC090iC04p06907.
- 1243 Talley, L.D., McCartney, M.S., 1982. Distribution and circulation of Labrador Sea Water. *Journal of*  
1244 *Physical Oceanography* 12, 1189-1205. doi: 10.1175/1520-  
1245 0485(1982)012<1189:DACOLS>2.0.CO;2.
- 1246 Tanhua, T., Olsson, K.A., Jeansson, E., 2005. Formation of Denmark Strait overflow water and its  
1247 hydro-chemical composition. *Journal of Marine Systems* 57, 3, 264-288. doi:  
1248 10.1016/j.jmarsys.2005.05.003.
- 1249 Tanhua, T., Olsson, K.A., Jeansson, E., 2008. Tracer evidence of the origin and variability of  
1250 Denmark Strait Overflow Water, in: Dickson, R.R., Jens, M., Rhines, P. (Eds.), *Arctic-  
1251 Subarctic Ocean Fluxes: Defining the Role of the Northern Seas in Climate*. Springer,  
1252 Science+Business Media B.V., P.O. Box 17, AA Dordrecht, The Netherlands, pp. 475-503.
- 1253 Thierry, V., De Boissésou, E., Mercier, H., 2008. Interannual variability of the Subpolar Mode  
1254 Water properties over the Reykjanes Ridge during 1990-2006. *Journal of Geophysical*  
1255 *Research* 113, C04016. doi: 10.1029/2007JC004443.

- 1256 Thompson, R.O., Edwards, R.J., 1981. Mixing and water-mass formation in the Australian  
1257 Subantarctic. *Journal of Physical Oceanography* 11, 10, 1399-1406. doi: 10.1175/1520-  
1258 0485(1981)011<1399:MAWMFI>2.0.CO;2.
- 1259 Tomczak, M., 1981. A multi-parameter extension of temperature/salinity diagram techniques for the  
1260 analysis of non-isopycnal mixing. *Progress in Oceanography* 10, 3, 147-171. doi:  
1261 10.1016/0079-6611(81)90010-0.
- 1262 Tomczak, M., 1999. Some historical, theoretical and applied aspects of quantitative water mass  
1263 analysis. *Journal of Marine Research* 57, 2, 275-303. doi: 10.1357/002224099321618227.
- 1264 Tomczak, M., Large, D.G., 1989. Optimum multiparameter analysis of mixing in the thermocline of  
1265 the eastern Indian Ocean. *Journal of Geophysical Research* 94, C11, 16141-16149. doi:  
1266 10.1029/JC094iC11p16141.
- 1267 Tsuchiya, M., Talley, L.D., McCartney, M.S., 1992. An eastern Atlantic section from Iceland  
1268 southward across the equator. *Deep Sea Research Part A. Oceanographic Research*  
1269 *Papers* 39, 11, 1885-1917. doi: 10.1016/0198-0149(92)90004-D.
- 1270 van Aken, H.M., 2000. The hydrography of the mid-latitude northeast Atlantic Ocean I: The deep  
1271 water masses. *Deep Sea Research Part I: Oceanographic Research Papers* 47, 5, 757-  
1272 788. doi: 10.1016/S0967-0637(99)00092-8.
- 1273 van Aken, H.M., Becker, G., 1996. Hydrography and through-flow in the north-eastern North  
1274 Atlantic Ocean: the NANSEN project. *Progress in Oceanography* 38, 4, 297-346. doi:  
1275 10.1016/S0079-6611(97)00005-0.
- 1276 van Aken, H.M., de Boer, C.J., 1995. On the synoptic hydrography of intermediate and deep water  
1277 masses in the Iceland Basin. *Deep Sea Research Part I: Oceanographic Research Papers*  
1278 42, 2, 165-189. doi: 10.1016/0967-0637(94)00042-Q.
- 1279 van Aken, H.M., de Jong, M.F., 2012. Hydrographic variability of Denmark Strait Overflow Water  
1280 near Cape Farewell with multi-decadal to weekly time scales. *Deep Sea Research Part I:  
1281 Oceanographic Research Papers* 66, 41-50. doi: 10.1016/j.dsr.2012.04.004.
- 1282 von Appen, W.-J., Koszalka, I.M., Pickart, R.S., Haine, T.W.N., Mastropole, D., Magaldi, M.G.,  
1283 Valdimarsson, H., Girton, J., Jochumsen, K., Krahnemann, G., 2014. The East Greenland  
1284 Spill Jet as an important component of the Atlantic Meridional Overturning Circulation.

- 1285 Deep Sea Research Part I: Oceanographic Research Papers 92, 75-84. doi: 10.1016/j.  
1286 dsr.2014.06.002.
- 1287 Willebrand, J., Barnier, B., Böning, C., Dieterich, C., Killworth, P.D., Le Provost, C., Jia, Y.,  
1288 Molines, J.-M., New, A.L., 2001. Circulation characteristics in three eddy-permitting models  
1289 of the North Atlantic. Progress in Oceanography 48, 123-161. doi: 10.1016/S0079-  
1290 6611(01)00003-9.
- 1291 Wüst, G., Defant, A., 1936. Atlas zur Schichtung und Zirkulation des Atlantischen Ozeans.  
1292 Wissenschaftliche Ergebnisse: Deutsche Atlantische Expedition auf dem Forschungs- und  
1293 Vermessungsschiff "Meteor" 1925-1927 6, Atlas, 103.
- 1294 Xu, X., Hurlburt, H.E., Schmitz Jr., W.J., Zantopp, R., Fischer, J., Hogan, P.J., 2013. On the  
1295 currents and transports connected with the atlantic meridional overturning circulation in the  
1296 subpolar North Atlantic. Journal of Geophysical Research 118, 502-516. doi:  
1297 10.1002/jgrc.20065.
- 1298 Xu, X., Schmitz Jr, W.J., Hurlburt, H.E., Hogan, P.J., Chassignet, E.P., 2010. Transport of Nordic  
1299 Seas overflow water into and within the Irminger Sea: An eddy-resolving simulation and  
1300 observations. Journal of Geophysical Research 115, C12048. doi: 10.1029/2010JC006351.
- 1301 Yashayaev, I., 2007. Hydrographic changes in the Labrador Sea, 1960-2005. Progress in  
1302 Oceanography 73, 3, 242-276. doi: 10.1016/j.pocean.2007.04.015.
- 1303 Yashayaev, I., Bersch, M., van Aken, H.M., 2007. Spreading of the Labrador Sea Water to the  
1304 Irminger and Iceland basins. Geophysical Research Letters 34, 10, L10602. doi:  
1305 10.1029/2006GL028999.
- 1306 Yashayaev, I., Dickson, R.R., 2008. Transformation and fate of overflows in the Northern North  
1307 Atlantic, in: Dickson, R.R., Jens, M., Rhines, P. (Eds.), Arctic-Subarctic Ocean Fluxes:  
1308 Defining the Role of the Northern Seas in Climate. Springer, Science+Business Media B.V.,  
1309 P.O. Box 17, AA Dordrecht, The Netherlands, pp. 505-526.
- 1310 Yashayaev, I., Holliday, N.P., Bersch, M., van Aken, H.M., 2008. The History of the Labrador Sea  
1311 Water: Production, Spreading, Transformation and Loss, in: Dickson, R.R., Jens, M.,  
1312 Rhines, P. (Eds.), Arctic-Subarctic Ocean Fluxes: Defining the Role of the Northern Seas in

1313 Climate. Springer, Science+Business Media B.V., P.O. Box 17, AA Dordrecht, The  
1314 Netherlands, pp. 569-612.  
1315

## Figure captions

Figure 1: Location of the 4x and OVIDE hydrographic stations plotted on bathymetry (500 m intervals). The North Atlantic circulation scheme, the major topographical features of the Subpolar North Atlantic, as well as the main water masses are also shown: East Greenland Current (EGC), West Greenland Current (WGC), Labrador Current (LC), Deep Western Boundary Current (DWBC), North Atlantic Current (NAC), Denmark Strait Overflow Water (DSOW), Iceland–Scotland Overflow Water (ISOW), Labrador Sea Water (LSW), Mediterranean Water (MW), North East Atlantic Deep Water (NEADW), Charlie–Gibbs Fracture Zone (CGFZ), Bight Fracture Zone (BFZ), Mid-Atlantic Ridge (M.A.R.) and Iberian Abyssal Plain (I.A.P.). Schematic diagram of the large-scale circulation compiled from Schmitz and McCartney (1993), Dengler et al. (2006), Schott and Brandt (2007, Plate 1), Sutherland and Pickart (2008, Fig. 16), Lherminier et al. (2010, Fig. 1b) and Sarafanov et al. (2012).

Figure 2: Mean (a) potential temperature ( $\theta$ ), (b) salinity, (c) oxygen, (d) nitrate, (e) silicate and (f) phosphate along the OVIDE section, from the Iberian Peninsula (right) to Greenland (left).

Figure 3: (A) Potential temperature ( $\theta$ )/Salinity (S)-diagram including the Source Water Types (Table 2) used in the analysis and (B) zoomed for bottom waters. The mixing *figures* are shown in the (C) legend (see Table 2 for the acronyms of the source water types). The isopycnals referenced in the chapter are also plotted, i.e.,  $\sigma_1 = 32.15$  and  $\sigma_1 = 32.42$  (where is  $\sigma_1$  potential density referenced to 1000 dbar).

Figure 4: Water mass distributions of the mean result for the OVIDE sections (2002–2010), from the Iberian Peninsula (right) to Greenland (left). The water mass contributions are expressed on a per unit basis (see Table 2 for the acronyms of the source water types). The dashed horizontal lines represent isopycnals:  $\sigma_1 = 32.15$ , which marks the limit between the upper and lower limb of the Atlantic Meridional Overturning Circulation (plot a); and  $\sigma_1 = 32.42$  (very similar to  $\sigma_0 = 27.8$ ), which marks the lower limit of Labrador Sea Water (LSW) on the classic works (plot e) and

approximately crosses the potential temperature/salinity definition of the source water type for LSW (Fig. 3a).  $\sigma_1 = 32.42$  has the advantage of not varying rapidly in the eastern half of the sections.

Figure 5: Water mass distributions along the WOCE A25 sections, from 1997 (4x section, upper plots) to 2010 (OVIDE section, lower plots), from the Iberian Peninsula (right) to Greenland (left). The water mass contributions are expressed on a per unit basis. Note that  $SPMW = IrSPMW + IcSPMW$ . The dashed white line on the DSOW plots represents the limit of the PIW contributions (5 % isoline) (see Table 2 for the acronyms of the source water types).

Figure 6: Net water mass volume transports perpendicular to the OVIDE section for the mean result of the period (2002–2010). Transports (in Sv;  $1 \text{ Sv} = 10^6 \text{ m}^3 \text{ s}^{-1}$ ) are positive northwards. Note that Central refers to Central Waters (see Table 2 for the acronyms of the source water types).

Figure 7: Schematic diagram of the water mass circulation, transformation and transports in the North Atlantic Subpolar Gyre, based on a two-layer box model in between the OVIDE sections and the Greenland–Iceland–Scotland sills (GISS). The transports (in Sv;  $1 \text{ Sv} = 10^6 \text{ m}^3 \text{ s}^{-1}$ ) at the southern boundary are the mean transports across the OVIDE sections as obtained in the present study. The transports at the northern boundary (GISS) are defined as explained in section 5. The boundary between the western (East North Atlantic (ENA) Basin) and eastern (Irminger Basin) boxes is the Reykjanes Ridge (RR). RR is closed (open) for the deep (upper-ocean and mid-depth) circulation. The diapycnal volume fluxes (crossed and point circles) and the transports across the RR are inferred from the condition of volume conservation. The uncertainties are shown in grey. Note that CW accounts for Central Waters and AW for Atlantic waters (see Table 2 for the acronyms of the source water types); I.P. for Iberian Peninsula.

Figure A3.1: Total residual from the extended Optimum MultiParameter (eOMP) analysis (a) and individual residuals from each eOMP equation: (b) potential temperature ( $\theta$ , in  $^{\circ}\text{C}$ ) and salinity (S);

(c) silicate ( $\text{SiO}_2$ ) and nitrate ( $\text{NO}_3$ ) (both in  $\mu\text{mol kg}^{-1}$ ); and (d) phosphate ( $\text{PO}_4$ ) and oxygen ( $\text{O}_2$ ) (both in  $\mu\text{mol kg}^{-1}$ ).

Figure 1

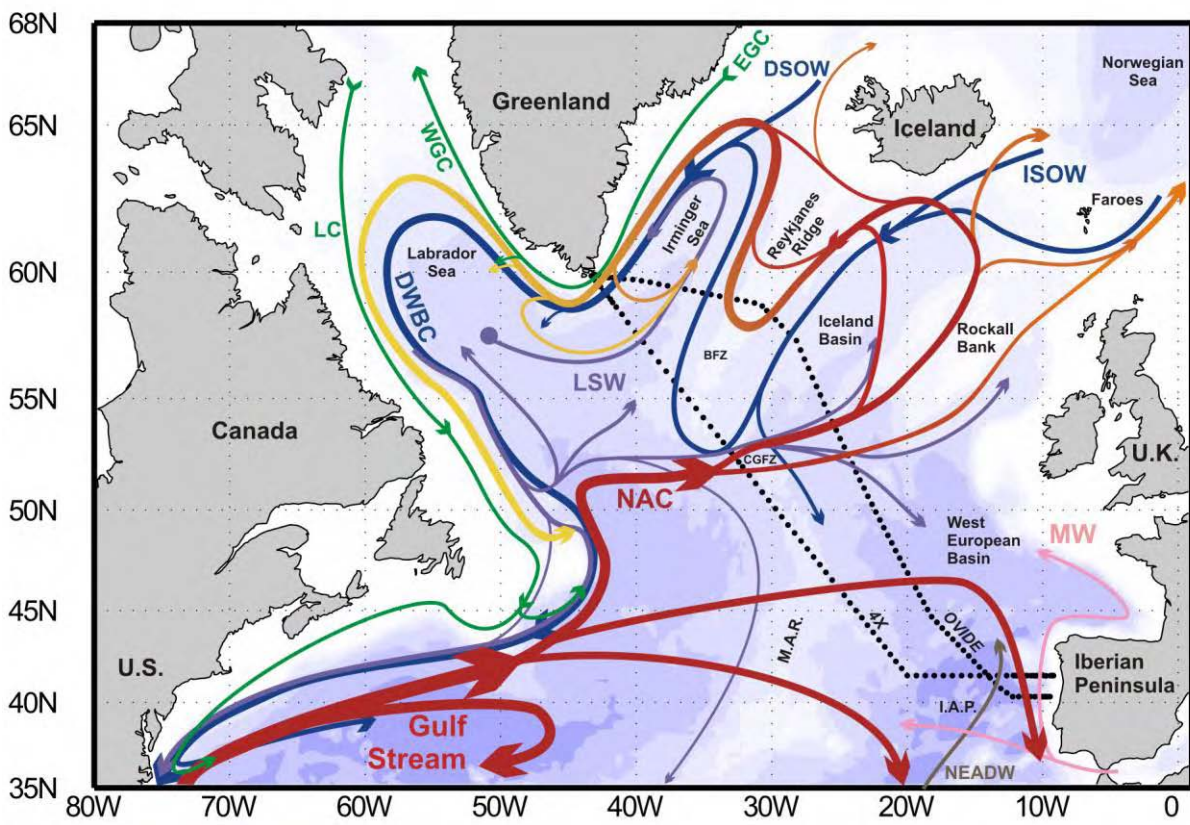


Figure 2

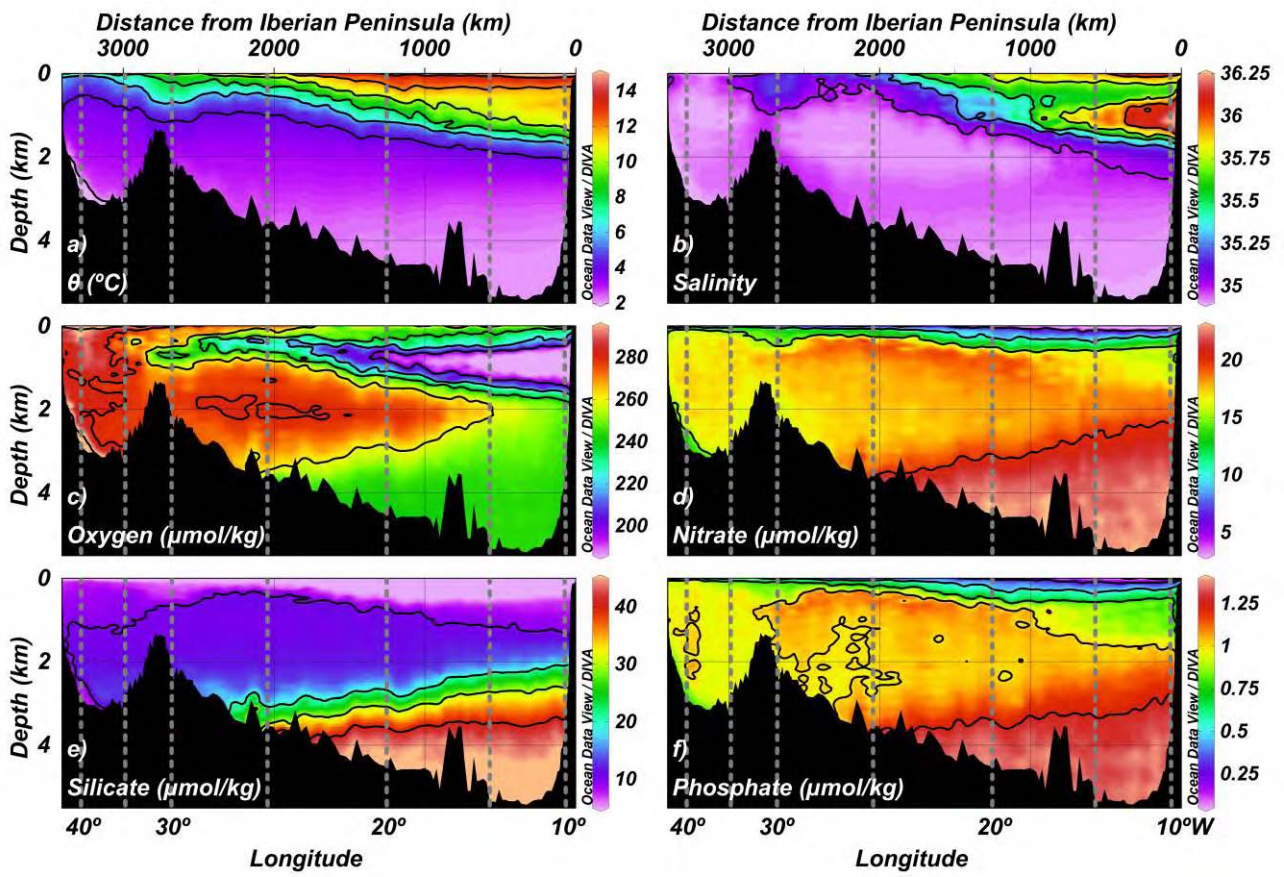


Figure 3

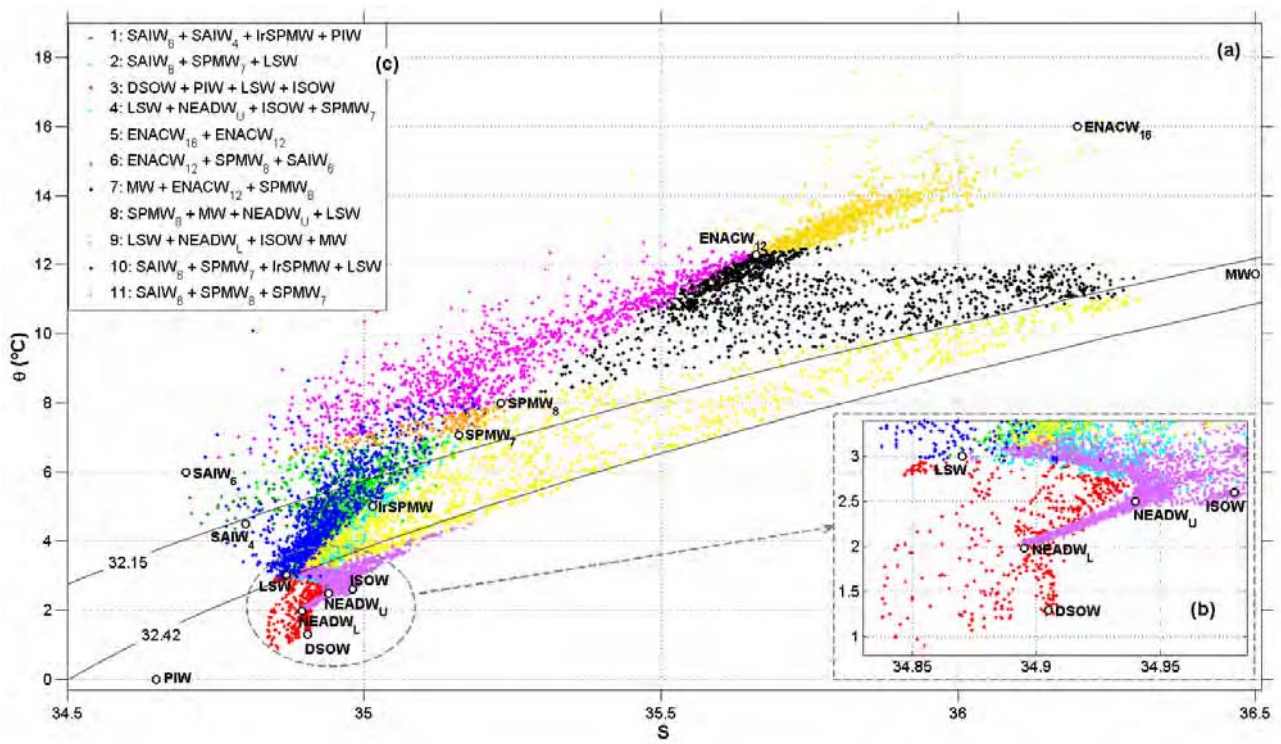


Figure 4

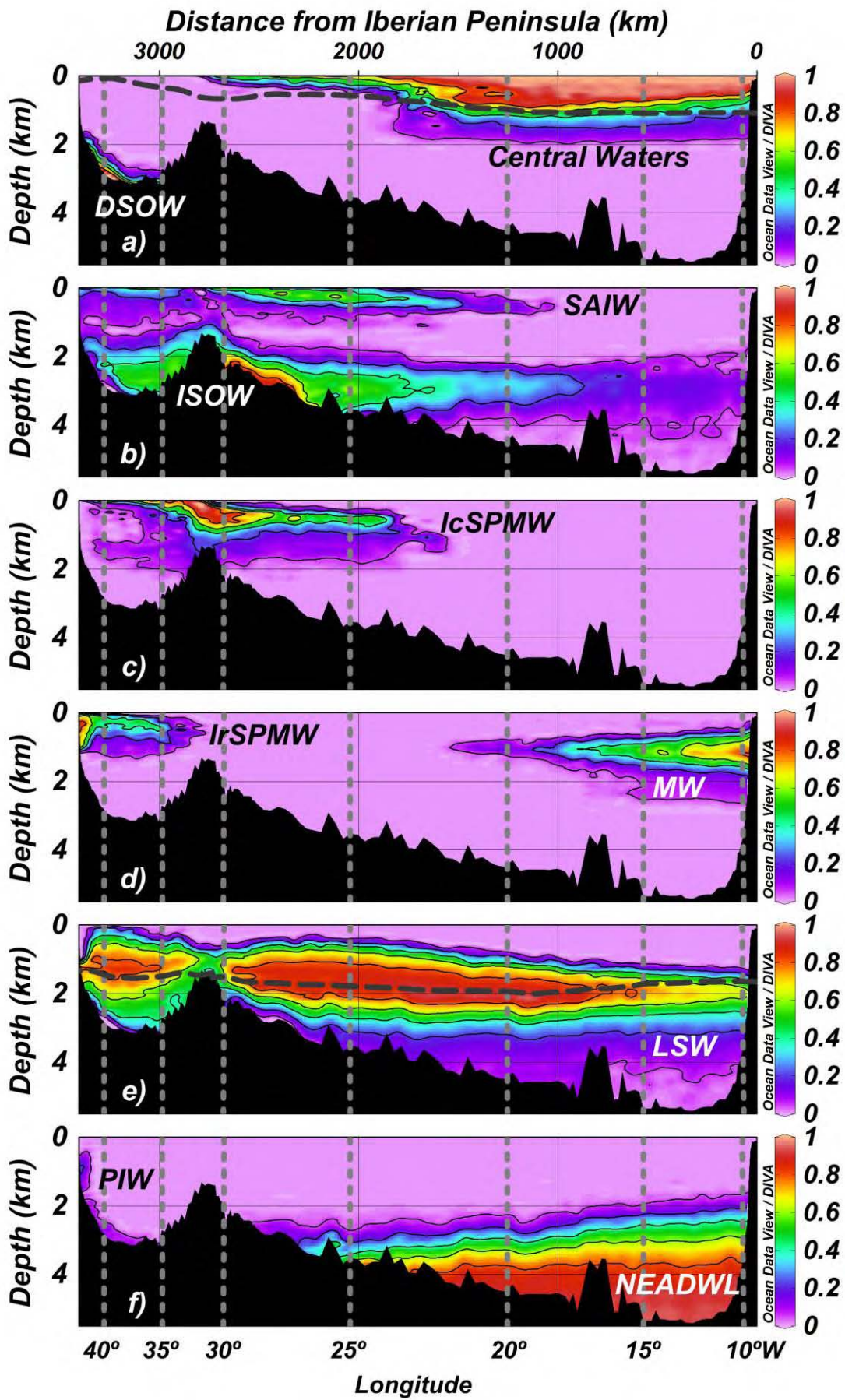


Figure 5

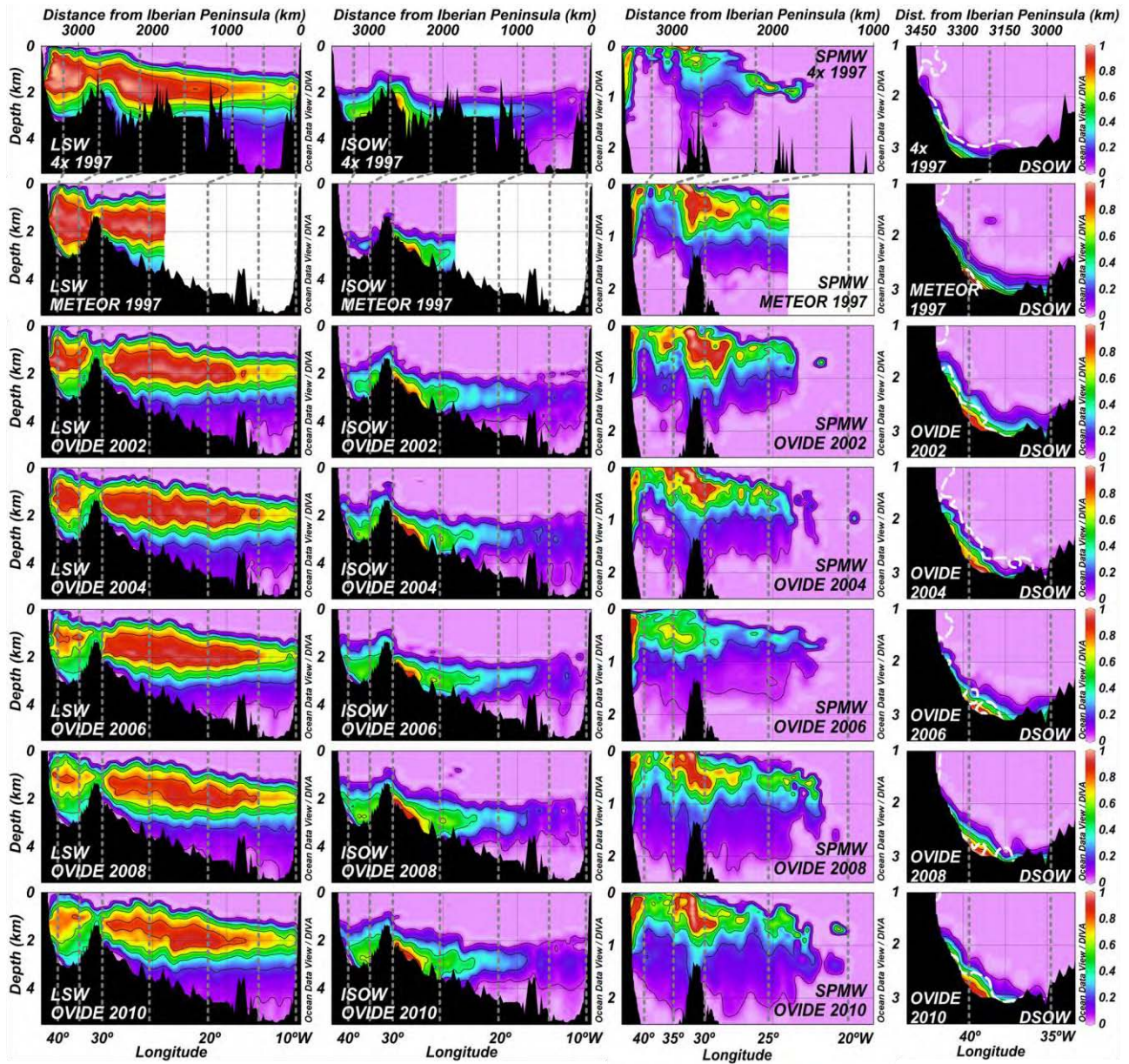


Figure 6

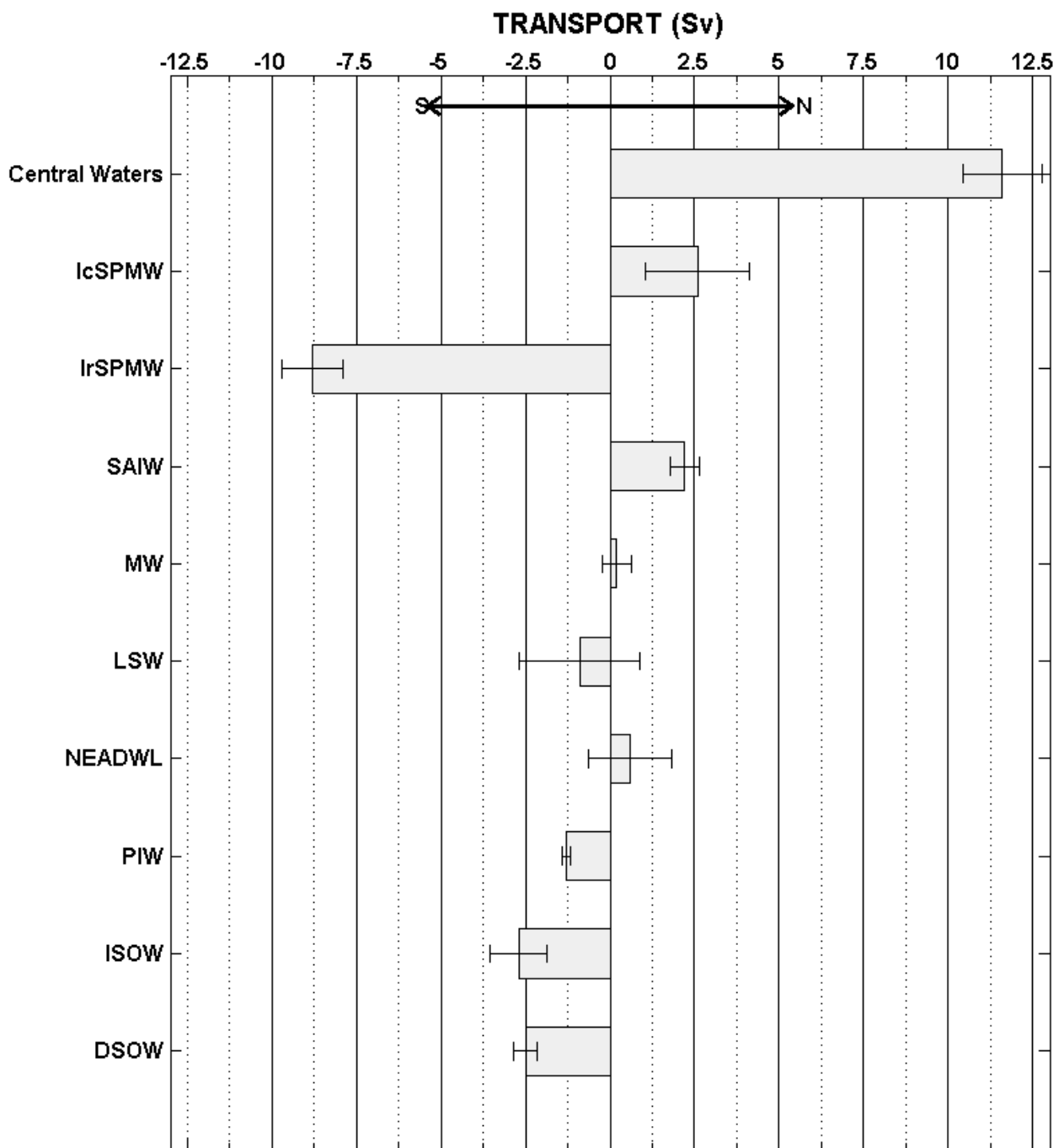


Figure 7

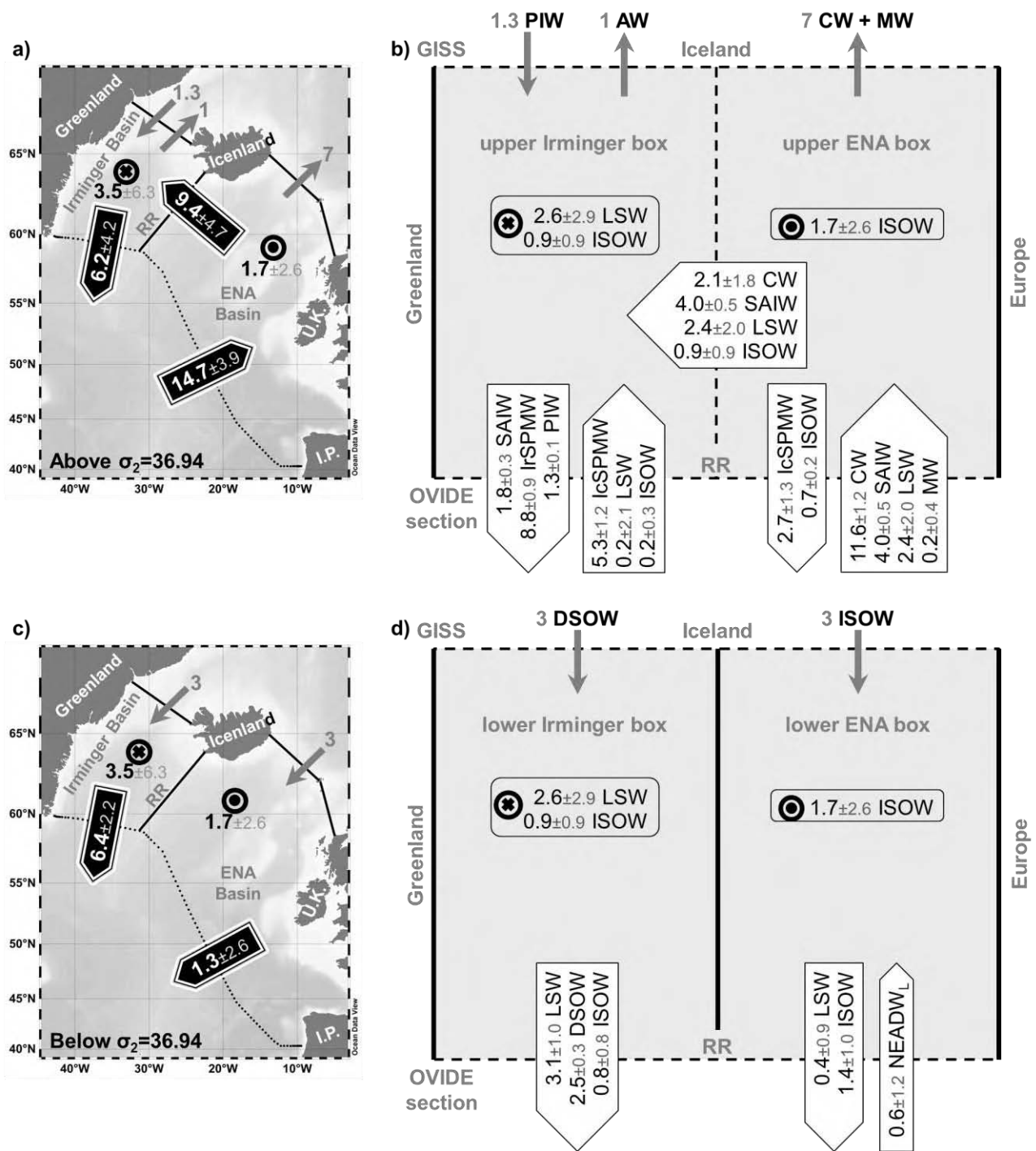


Figure A3.1

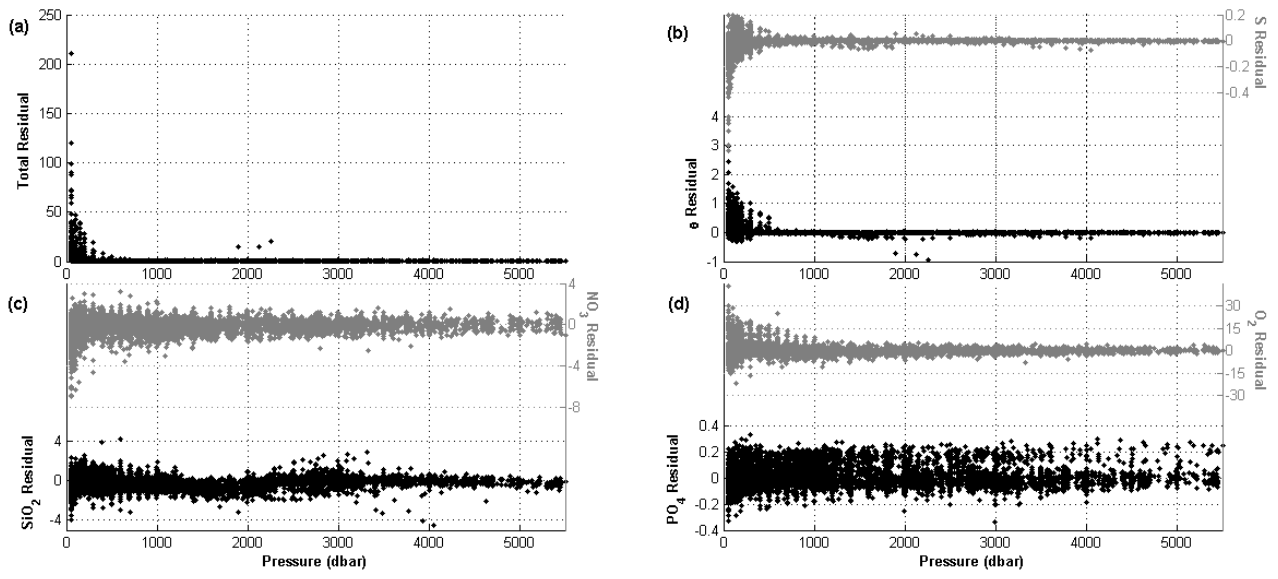


Table 1: Hydrographic cruises.

Cruise Name	Month/Year	Vessel	Reference
METEOR 1997	08-09/1997	R/V Meteor	Rhein et al. (2002)
4x 1997	08-09/1997	R/V Discovery	Álvarez et al. (2002)
OVIDE 2002	06-07/2002	N/O Thalassa	Lherminier et al. (2007)
OVIDE 2004	06-07/2004	N/O Thalassa	Lherminier et al. (2010)
OVIDE 2006	05-06/2006	R/V Maria S. Merian	Gourcuff et al. (2011)
OVIDE 2008	06-07/2008	N/O Thalassa	Mercier et al. (2013)
OVIDE 2010	06-07/2010	N/O Thalassa	Mercier et al. (2013)

Table 2: Main properties of each of the Source Water Types (SWTs) considered in the study with their corresponding standard deviation. The weights of each equation are also given, together with the square of correlation coefficients ( $r^2$ ) between the observed and estimated properties, the Standard Deviation of the Residuals (SDR) and the SDR/ $\epsilon$  ratios from the data below 400 dbar. The  $\epsilon$  used to compute the SDR/ $\epsilon$  ratios are the accuracies of the measured properties listed in Appendix A2. The last column accounts for the uncertainties in the SWTs contributions. Values expressed on a per one basis.

	Potential temperature ( $\theta^{SWT}$ ) °C	Salinity ( $S^{SWT}$ )	Silicate ( $SiO_2^{SWT}$ ) $\mu\text{mol kg}^{-1}$	Nitrate ( $NO_3^{SWT}$ )	Phosphate ( $PO_4^{SWT}$ )	Oxygen ( $O_2^{SWT}$ )	Uncertainty
ENACW <sub>16</sub>	16.00±0.13	36.20±0.02	0.85±0.12	0.00±0.16	0.00±0.01	241±7	0.04
ENACW <sub>12</sub>	12.30±0.18	35.66±0.03	1.6±0.8	7±1	0.31±0.07	251±8	0.04
MW	11.7±0.2	36.500±0.011	4.88±0.15	10.9±0.2	0.70±0.03	210±8	0.015
SAIW <sub>6</sub>	6.0±0.2	34.70±0.03	6.3±2.2	13±1	0.86±0.07	287±9	0.04
SAIW <sub>4</sub>	4.5±0.2	34.80±0.03	1.4±2.2	0±1	0.05±0.07	290±9	0.05
SPMW <sub>8</sub>	8.00±0.11	35.230±0.016	3.2±2.2	11±1	0.68±0.01	289±6	0.07
SPMW <sub>7</sub>	7.07±0.07	35.160±0.006	5.38±0.16	13.70±0.16	1.06±0.01	280±9	0.08
IrSPMW	5.00±0.02	35.014±0.013	7.1±0.4	15.0±0.4	0.98±0.02	300±9	0.13
LSW	3.00±0.19	34.87±0.02	10.0±0.8	16.5±0.8	1.05±0.12	287±10	0.10
ISOW	2.60±0.08	34.980±0.003	10±1	15.5±0.6	1.20±0.04	289±10	0.08
DSOW	1.30±0.06	34.905±0.006	7.8±0.5	14.1±0.8	1.10±0.06	309±10	0.05
PIW	0.0±0.2	34.65±0.03	8.4±2.2	9±1	0.25±0.07	310±11	0.06
NEADW <sub>U</sub>	2.50±0.08	34.940±0.007	29.2±0.6	19.2±0.6	1.32±0.05	269±10	-
NEADW <sub>L</sub>	1.98±0.03	34.895±0.003	48.0±0.4	22.6±0.5	1.50±0.04	252±10	0.02
Weights	20	10	2	3*	2*	2	
$r^2$	0.9991	0.9891	0.9975	0.9784	0.9477	0.9926	
SDR	0.02	0.006	0.5	0.5	0.07	2	
SDR/ $\epsilon$	2	1	2	3	3	2	

\* The weights for NO and PO are the same as for  $NO_3^0$  and  $PO_4^0$ , respectively.

\*\*  $O_2$  and nutrients represent preformed values; note that  $O_2$  values are close to saturation and nutrient values are low.

\*\*\* ENACW<sub>16</sub> and ENACW<sub>12</sub> = Eastern North Atlantic Central Waters; MW = Mediterranean Water; SAIW<sub>6</sub> and SAIW<sub>4</sub> = Subarctic Intermediate Waters; SPMW<sub>8</sub> and SPMW<sub>7</sub> = Subpolar Mode Waters of the Iceland Basin and IrPMW = of the Irminger Basin; LSW = Labrador Sea Water; ISOW = Iceland-Scotland Overflow Water; DSOW = Denmark Strait Overflow Waters; PIW = Polar Intermediate Water; and NEADW<sub>U</sub> = North East Atlantic Deep Water upper and NEADW<sub>L</sub> = lower.

\*\*\*\* NEADW<sub>U</sub> has no uncertainty value since it is considered as a composed SWT (MW + LSW + ISOW + NEADW<sub>L</sub>, see section 3).